Unimolecular reaction rate theory for transition states of partial looseness. II. Implementation and analysis with applications to NO_2 and C_2H_6 dissociations

David M. Wardlaw[a] and R. A. Marcus
Arthur Amos Noyes Laboratory of Chemical Physics, California Institute of Technology,[b] Pasadena, California 91125

(Received 22 April 1985; accepted 6 June 1985)

Implementation of RRKM theory for unimolecular dissociations having transition states of any degree of looseness is described for reactions involving dissociation into two fragments. The fragments may be atomic, diatomic, or polyatomic species. Action-angle and internal coordinates for the transitional modes of the reaction, transformations to Cartesian coordinates, and other calculational aspects are described. Results for the $NO_2 \rightarrow NO + O$ reaction are presented, including the dependence of the microcanonical rate constant on the bond fission and bending potentials for model potential energy surfaces. Illustrative calculations for the $C_2H_6 \rightarrow 2CH_3$ reaction are also given.

I. INTRODUCTION

Frequently the transition state of a reaction is defined in terms of the position of some maximum (saddle point) in the potential energy surface along the reaction coordinate. However, in reactions such as certain unimolecular dissociations to free radicals (and, hence, recombination of free radicals) and some ion–molecule reactions, a local potential energy barrier maximum may be absent. A method was presented in part I[1] for implementing RRKM theory for such reactions, and it was illustrated for the dissociation $H_2O_2 \rightarrow 2OH$. In the present paper the coordinates, the transformations between coordinate systems, and the evaluation of the phase space integral arising in this formulation are described in some detail. Illustrative results are given for the reactions $NO_2 \rightarrow NO + O$ and $C_2H_6 \rightarrow 2CH_3$.

The rate constant k_{EJ} of a unimolecular reaction is given in RRKM theory[2] as a function of the energy E of the molecule (in the center-of-mass frame) and of the total angular momentum J,

$$k_{EJ} = \frac{N_{EJ}}{h\rho_{EJ}}, \tag{1}$$

where N_{EJ} is the number of quantum states of the transition state having at the given J an energy less than or equal to E in all degrees of freedom but the reaction coordinate, and ρ_{EJ} is the density of states of the dissociating or isomerizing molecule. Tunneling corrections along the reaction coordinate and any reaction path degeneracy can be introduced into N_{EJ} if needed.[3] A unimolecular rate constant at any pressure is obtained from Eq. (1) in the standard way by suitably weighting the contributions from different E's and J's [Eq. (4) of Ref. 4]. The main idea for calculating N_{EJ}, described in part I, is that the degrees of freedom are subdivided into "transitional" ones and the remaining coordinates, in a center-of-mass system of coordinates. The transitional degrees of freedom involve (a) the bending motions of the two parts of the dissociating molecule, which become free rotations in the products, (b) the relative orbital motion of the separating fragments, and (c) the other coordinates, if any, which change considerably their form of motion during the progress of the molecule along the reaction coordinate. These various motions are typically strongly coupled to each other and are constrained by energy and total angular momentum conservation. Such coupling and constraints make a purely quantum mechanical calculation of the energy levels of the system at each value of the reaction coordinate formidable. The contribution $\Omega_J(\epsilon)$ of such coordinates to N_{EJ} as a function of their energy E can be calculated from an evaluation of the corresponding classical phase space integral, introducing quantum corrections[3] if necessary.

With this subdivision of the coordinates into two groups N_{EJ} can be written as[1]

$$N_{EJ} = \int_0^{E'} N_V(E' - \epsilon)\Omega_J(\epsilon)d\epsilon, \tag{2}$$

where $\Omega_J(\epsilon)d\epsilon$ is the number of quantum states of the transitional modes for the given J when their total energy lies in the interval $(\epsilon, \epsilon + d\epsilon)$, $N_V(E' - \epsilon)$ is the number of quantum states in the remaining coordinates when their energy is less than or equal to $E' - \epsilon$, E' being the available energy, i.e., E minus the value of the potential energy minimum at the given value of the reaction coordinate and minus the zero point energy of the modes included in N_V. The two types of coordinates are taken to be uncoupled from each other in Eq. (2), apart from an indirect coupling via the dependence of the molecular constants on the reaction coordinate. The value of N_V in Eq. (2) is obtained by the usual quantum count, while $\Omega_J(\epsilon)$ and N_{EJ} are evaluated by Monte Carlo methods. The minimum value of N_{EJ} along the reaction coordinate is then used to define the transition state[5] and, thereby, the value of N_{EJ} to be introduced for the numerator in Eq. (1). The quantity $\Omega_J(\epsilon)$ itself can be evaluated either by using action-angle variables, as in part I, or by using constrained internal coordinates. In the present paper the former are used.

The application of RRKM theory described in part I and in this paper foregoes the considerable simplicity afforded by largely analytical expressions[4,6] for N_{EJ}, in favor of a

[a] Present address: Department of Chemistry, Queens University, Kingston, Ontario, K7L 3N6 Canada.
[b] Contribution No. 7186.

 0021-9606/85/193462-19$02.10

more accurate physical treatment of the transition state for this more general case. The principal ingredients for calculating N_{EJ}, apart from the quantum count of N_V involve some tedious though relatively straightforward and readily programmed transformations and a Monte Carlo calculation. The results serve to identify the more important parts of the potential energy surface for the reactions concerned. They can be used as a basis for selecting suitable points for the calculation of improved potential energy surfaces for studying the rates of these reactions.

The present article is subdivided as follows: In Sec. II and the Appendices, the action-angle coordinates are given for the transitional modes, together with the transformations to the internal or relative coordinates. The subsequent evaluation of N_{EJ} is discussed in Sec. III and details of the Monte Carlo sampling, integration limits in the calculation of $\Omega_J(\epsilon)$, and the counts used for N_V are given in an Appendix. The theory is applied to the $NO_2 \rightarrow NO + O$ reaction in Sec. IV for a model potential surface (Appendix A), and compared with the theoretical results from the statistical adiabatic-channel model (SACM). The effect on N_{EJ} (and hence on k_{EJ}) of varying the bending and bond-fission potential energy functions is also investigated for this reaction. The potential energy surface used and the transformation from action-angle to internal coordinates for the $H_2O_2 \rightarrow 2$ OH reaction studied in part I are given in Appendices. Some illustrative results for the k_{EJ} of the $C_2H_6 \rightarrow 2CH_3$ reaction are given in Sec. V. A full account of the present treatment applied to this reaction, and comparisons with experimental data, are given later.[7] The C_2H_6 coordinate transformations and the methods given here are applicable to more general systems with larger polyatomic fragments. The N_{EJ} calculations of Secs. IV and V are discussed in Sec. VI and conclusions follow in Sec. VII.

II. ACTION-ANGLE VARIABLES, INTERNAL COORDINATES, AND DENSITY OF STATES

To calculate $\Omega_J(\epsilon)$ in Eq. (2) two sets of body-fixed coordinate axes are first defined, each fixed in a separating fragment.[1,8,9] The origin of each system is located at the center of mass of that fragment, and when either fragment has some symmetry its coordinate axes are chosen to coincide with its symmetry axes. A third set of body-fixed coordinates is also defined, fixed in the molecule as a whole. For the coordinates of the transitional modes the action-angle coordinates described previously[1,8–10] are then introduced. In the following and in Appendices, the action-angle variables are defined for three different classes of reacting systems of increasing complexity, represented by the reactions $NO_2 \rightarrow NO + O$, $H_2O_2 \rightarrow 2OH$, and $C_2H_6 \rightarrow 2CH_3$. The transformation of the action-angle variables to internal displacement plus separation distance coordinates, in which the potential energy function is usually expressed, is also described. These three reactions have two, four, and six transitional modes, respectively, and are prototypes for dissociation into an atom and a linear fragment, into two linear fragments, and into two nonlinear fragments.

Angular momentum action-angle variables for a nonlinear system such as $ABC \rightarrow AB + C$ (e.g., $NO_2 \rightarrow NO + O$) can be chosen to be j, j_z, l, l_z (written here and throughout in units of $\hbar = 1$)[11] and their conjugate angles α_j, β_j α_l, β_l. (Two distances and their conjugate momenta complete the set of variables in the center-of-mass system of coordinates.) The angles range over a 2π interval. The variables j and j_z describe the rotational angular momentum and the space-fixed z component of the diatomic AB, respectively; l and l_z denote the orbital angular momentum of the fragments and its z component. The conjugate angles are angle variables in the planes perpendicular to the corresponding angular momentum vectors. It is convenient to use instead the variables (J,α,J_z,β) obtained in a canonical transformation[9,10]

$$(j_z,\beta_j,l_z,\beta_l) \rightarrow (J,\alpha,J_z,\beta), \tag{3}$$

where $J(=|\mathbf{j}+\mathbf{l}|)$ is the action for the total angular momentum, J_z is its space-fixed component, and α, β are their respective conjugate angles. For a system so described and for a given value of J the semiclassical value Ω_J of quantum states of the transitional modes is

$$\Omega_J(\epsilon) = (2\pi)^{-4}\sigma^{-1}\int \cdots \int \times dJ_z\, dj\, dl\, d\alpha\, d\beta\, d\alpha_j\, d\alpha_l\, \Delta(J,j,l)\delta(\epsilon - H_{cl}) \tag{4}$$

(in units of $\hbar = 1$). Here, H_{cl} is the classical Hamiltonian for the transitional modes and is given below. $\Delta(J,j,l)$ is unity when the triangle inequality $|j-l| \leqslant J \leqslant j+l$ is fulfilled and zero otherwise. The integration limits for the angle variables are $(0, 2\pi)$. σ is a symmetry number which corrects for the overcounting of any indistinguishable configurations in these $(0, 2\pi)$ angle intervals. The angular momentum actions j and l are restricted by energy conservation and the limits on the J_z integral are $(-J,J)$.

The Hamiltonian H_{cl} for the transitional modes is written as

$$H_{cl} = \frac{j^2}{2\mu_{AB}r^2} + \frac{l^2}{2\mu R^2} + V_t(r_{AB\text{-}C},\theta), \tag{5}$$

where μ_{AB} is the reduced mass of AB, μ is the reduced mass for the relative motion of AB and C, and R is the distance between C and the center of mass of AB. The potential V_t for the transitional modes is modeled in the present study so as to be a function of the internal coordinates $r_{AB\text{-}C}$ and θ depicted in Fig. 1(a). The other coordinate r in Fig. 1(a) corresponds to the AB bond length and that vibration contributes instead to the quantum state count in $N_V(E' - \varepsilon)$. The reaction coordinate R, the angular momenta j and l, and the angle γ between $\mathbf{R}$ and $\mathbf{r}$ are depicted in Fig. 1(b). The functional form and numerical parameters used for V_t are given in Appendix A and for more complex systems in Appendices B and C.

To evaluate V_t in Eq. (5), the internal coordinates, $r_{AB\text{-}C}$ and θ are first expressed in terms of the Jacobi coordinates (R, r, γ) as in Appendix A. For any R, r is then replaced by its R-dependent equilibrium value r_e (Appendix A), and γ is expressed in terms of J and the action-angle variables appearing in Eq. (4):

$$\cos\gamma = \cos\alpha_j \cos\alpha_l + \sin\alpha_j \sin\alpha_l \cos\theta_{lj}, \tag{6}$$

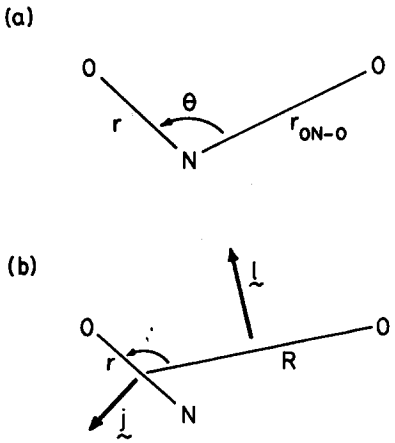

FIG. 1. (a) The N–O length r, the bond dissociation coordinate r_{ON-O}, and the bending angle θ for the $NO_2 \rightarrow NO + O$ system. (b) Angular momenta for the NO fragment rotation and for the orbital motion of ON and O; R is the distance between the centers of mass, and γ is the angle between **r** and **R**.

where θ_{lj} is the angle between **l** and **j** and is given as a function of l, j, and J in Table II. The angles γ, α_j, and α_l are depicted in Fig. 2 and, together with other angles, are specified in Tables I and III. The form of Eq. (6) applies to the various other systems of angles used in this paper and such results systematically follow from the identity[12]

$$(\mathbf{a}\times\mathbf{b})\cdot(\mathbf{c}\times\mathbf{d}) = (\mathbf{a}\cdot\mathbf{c})(\mathbf{b}\cdot\mathbf{d}) - (\mathbf{a}\cdot\mathbf{d})(\mathbf{b}\cdot\mathbf{c}), \tag{7}$$

with **a**, **b**, **c**, and **d** identified in Table III.

In the above way V_t, and hence H_{cl}, are specified by the variables $(R,r,J,j,l,\alpha_j,\alpha_l)$. The latter determine only the relative positions of the atoms. Hence, V_t and H_{cl} are independent of the variables (J_z,α,β), which determine the overall orientation of the body-fixed frame,[10] permitting the integral in Eq. (4) to be simplified to

$$\Omega_J(\epsilon) = (2J+1)(2\pi)^{-2}\sigma^{-1}\int\cdots\int \times dj\, dl\, d\alpha_j\, d\alpha_l \Delta(J,j,l)\delta(\epsilon - H_{cl}), \tag{8}$$

which, combined with Eq. (2), yields

TABLE I. Definition of Euler angles conjugate to various angular momenta.[a]

System	Angular momentum	Conjugate angle	Reference axis x	Rotated axis y
NO_2	l	α_l	$\mathbf{l}\times\mathbf{j}$	$\mathbf{R}$
	j	α_j	$\mathbf{l}\times\mathbf{j}$	$\mathbf{r}$
H_2O_2	l	α_l	$\mathbf{l}\times\mathbf{k}$	$\mathbf{R}$
	k	α_k	$\mathbf{l}\times\mathbf{k}$	$\mathbf{j}_1\times\mathbf{j}_2 = \mathbf{j}_1\times\mathbf{k}$
	j_i	α_i	$\mathbf{j}_1\times\mathbf{j}_2$	$\mathbf{r}_i$
C_2H_6	l	α_l	$\mathbf{l}\times\mathbf{k}$[b]	$\mathbf{R}$
	k	α_k	$\mathbf{l}\times\mathbf{k}$[b]	$\mathbf{j}_1\times\mathbf{j}_2 = \mathbf{j}_1\times\mathbf{k}$
	j_i	α_i	$\mathbf{l}\times\mathbf{j}_i$[c]	$\kappa_i\times\mathbf{j}_i$
	κ_i	γ_i	$\kappa_i\times\mathbf{j}_i$[d]	$\mathbf{e}_{x_i''}$

[a] All angles range from 0 to 2π and are obtained by counter-clockwise rotation about $\mathbf{x}\times\mathbf{y}$ from **x** to **y** (Ref. 12). The subscript i refers to fragment 1 or 2.
[b] Corresponds to axis **x** in Fig. 4(a).
[c] Corresponds to the line of nodes N_1' in Fig. 4(a) for $i = 1$.
[d] Corresponds to the line of nodes N_1'' in Fig. 4(a) for $i = 1$.

$$N_{EJ} = (2J+1)(2\pi)^{-2}\sigma^{-1}\int\cdots\int \times dj\, dl\, d\alpha_j\, d\alpha_l\, N_V(E' - H_{cl})\Delta(J,j,l), \tag{9}$$

the desired relation. In Eq. (9) $N_V(E' - H_{cl})$ is zero when $E' < H_{cl}$. The evaluation of the integral in Eq. (9) is described in Sec. III.

The foregoing equations and concepts are extended to more complex reacting systems in Appendices D and E. Various relevant angles are depicted in Figs. 3 and 4. The case of $J = 0$ is typically unimportant, since it is only one point on a distribution of many J's. Nevertheless, it is given for completeness in Appendix G for the various systems.

III. EVALUATION OF N_{EJ}

In evaluating the integral for N_{EJ} appearing in Eq. (9) [and in Eqs. (D9) and (E8)] by analytical or quadrature methods one encounters relatively high dimensionality (4 to 12), interdependent integration limits, and an integrand in which

TABLE II. Definitions of angles contained between various angular momenta.[a]

System	Angular momentum pair	Angle χ	$\cos\chi$
NO_2	(l,j)	θ_{lj}	$(J^2 - l^2 - j^2)/2lj$
H_2O_2, C_2H_6	(l,k)	θ_{lk}	$(J^2 - l^2 - k^2)/2lk$
	(j_1,j_2)	θ_{12}	$(k^2 - j_1^2 - j_2^2)/2j_1j_2$
	(k,j_1)	θ_{k1}	$(j_1^2 + k^2 - j_2^2)/2j_1k$
	(k,j_2)	θ_{k2}	$(j_2 + k^2 - j_1^2)/2j_2k$
	(l,j_1)	θ_{l1}	$\cos\theta_{lk}\cos\theta_{k1} + \sin\theta_{lk}\sin\theta_{k1}\cos\alpha_k$[b]
	(l,j_2)	θ_{l2}	$\cos\theta_{lk}\cos\theta_{k2} - \sin\theta_{lk}\sin\theta_{k2}\cos\alpha_k$[b]

[a] In all cases $0<\theta<\pi$ and $\sin\theta$ is obtained from $\cos\theta$ as the positive root.
[b] These expressions are obtained from Eq. (7) with $\mathbf{a} = \mathbf{l}$, $\mathbf{b} = \mathbf{d} = \mathbf{k}$, and $\mathbf{c} = \mathbf{j}_i$; the sign difference arises because α_k is the angle between $\mathbf{l}\times\mathbf{k}$ and $\mathbf{j}_1\times\mathbf{k} = \mathbf{j}_1\times\mathbf{j}_2$ (see Table I), whereas $\pi + \alpha_k$ is the angle between $\mathbf{l}\times\mathbf{k}$ and $\mathbf{j}_2\times\mathbf{k} = -\mathbf{j}_1\times\mathbf{j}_2$.

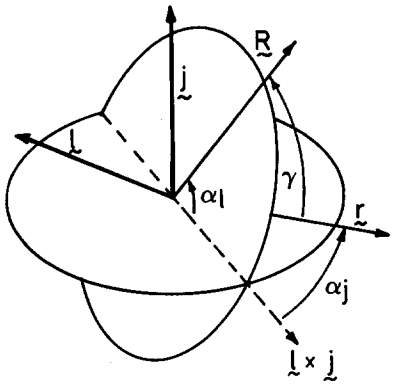

FIG. 2. An Euler diagram depicting the various angles involved in describing the transitional degrees of freedom for an atom plus diatom system. The planes in which **R** and **r** lie are perpendicular to **l** and **j**, respectively. The two planes intersect along the line of nodes **l**×**j**. α_l and α_j are angles conjugate to l and j, respectively, and γ is the angle between **R** and **r**. For pictorial clarity the angle θ_{lj} between **l** and **j** is not shown. All Euler angles are defined by a right-hand rule, i.e., they describe a counterclockwise rotation in the plane perpendicular to the axis of rotation.

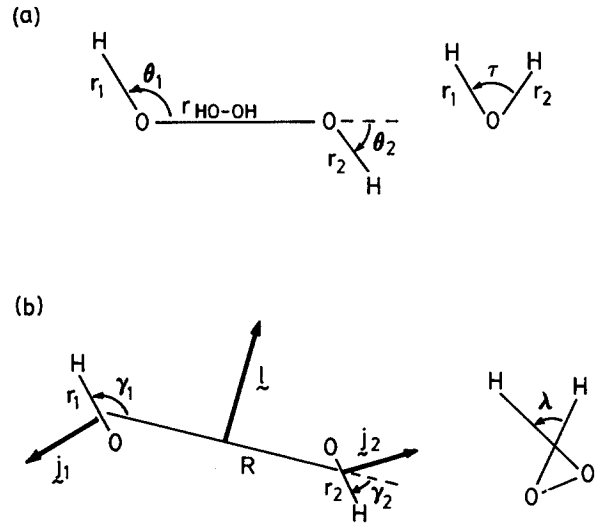

FIG. 3. (a) The OH bond lengths r_1 and r_2, bond dissociation coordinate r_{OH-OH}, bending angles θ_1 and θ_2, and torsional angle τ for the $H_2O_2 \rightarrow 2OH$ system. (b) Angular momenta for fragment rotations and for the relative motion of HO· · ·OH, the distance R between the centers of mass, the angles γ_1 between **R** and $\mathbf{r}_i$ ($i = 1, 2$), and the angle λ between the plane defined by $\mathbf{r}_1$ and **R** and that defined by $\mathbf{r}_2$ and **R**.

all variables of integration are coupled via V_t, which itself is a complicated function of the new variables. Such integrals are well suited to evaluation by Monte Carlo methods.[13] One may write

$$N_{EJ} = N_{EJ}^{MC} \pm \sigma^{MC}, \tag{10}$$

where N_{EJ}^{MC} and $(\sigma^{MC})^2$ are Monte Carlo estimates of N_{EJ} and of the variance σ^2 of N_{EJ}^{MC}, respectively.

In this paper, which is aimed mainly at examining the salient features of the present method, we have found it expedient to use the crude Monte Carlo method for evaluating N_{EJ}^{MC} and σ^{MC}, namely to use a uniform sampling of all variables, combined with a weighting method[13] for coping with the awkward interdependent integration limits. The details of the calculation, including the counts for N_V, are given in Appendix F. Also described are some elementary procedures which reduced the variance $(\sigma^{MC})^2$ for the transitional modes. Other more sophisticated Monte Carlo techniques for evaluating N_{EJ} can, of course, also be used.

Monte Carlo calculations of phase space volumes have been used in completely classical calculations of numbers of states, densities of states, and unimolecular rate theory. Both rotating[14] and nonrotating[15–18] systems have been so studied, although for the rotating systems[14] the ensembles were not J fixed. In a study[17] of the vibrational predissociation of the Ar–BCl_3 van der Waals' molecule a generalization[15(b)] of Slater theory was used to obtain k_E's via Metropolis sampling. A similar approach was used[18] in a study of the unimolecular dissociation of methane. The results for $CH_4 \rightarrow CH_3 + H$ were converged, though an uncertainty of $\sim 100\%$ was reported for the Monte Carlo estimates of k_E for $CH_4 \rightarrow CH_2 + H_2$, due to the excessive computational times needed for convergence.

TABLE III. Identification of vectors used to define cosines of various angles via Eq. (7).

System	Angle	a	b	c	d
NO_2	γ	**l**×**j**	**r**	**l**×**j**	**R**
H_2O_2	λ	$\mathbf{r}_1$	**R**	$\mathbf{r}_2$	**R**
	φ	$\mathbf{j}_1 \times \mathbf{j}_2$	$\mathbf{r}_1$	$\mathbf{j}_1 \times \mathbf{j}_2$	$\mathbf{r}_2$
	γ_i	$\mathbf{j}_1 \times \mathbf{j}_2$	$\mathbf{r}_i$	**l**×**k**	**R**
	θ_R	**l**×**k**	**R**	**l**×**k**	$\mathbf{j}_1 \times \mathbf{j}_2$
	θ_{r_i}	$\mathbf{j}_1 \times \mathbf{j}_2$	$\mathbf{r}_i$	**l**×**k**	$\mathbf{j}_1 \times \mathbf{j}_2$
C_2H_6	β_i	**l**	**k**	**l**	$\mathbf{j}_i$

IV. RESULTS FOR THE REACTION $NO_2 \rightarrow NO + O$

A. Calculations for N_{EJ} vs E and J and comparison with SACM

Results for N_{EJ}, the quantity useful for assessing the accuracy and computational facility of the present method, are described in this section. Using a model potential energy surface described in Appendix A, results for N_{EJ} [with $\sigma = 1$ in Eq. (9)] were obtained for several J's and are plotted in Fig. 5 vs E'_∞, the energy of the separated products in excess of their zero point and potential energy.

To obtain N_{EJ} at the "bottleneck" value of R, $R^\dagger$, i.e., at the location of the minimum in the reactive flux, the integral in Eq. (9) was evaluated as a function of R at fixed intervals (0.1 Å for this reaction) using the Monte Carlo method described in Sec. III and Appendix F. The accuracy of the present Monte Carlo estimates of N_{EJ} as measured by σ^{MC}/N_{EJ}^{MC}, was at worst $\sim 1.5\%$ for all values of R. The relative accuracy was found to depend only on the number of integration points and was essentially independent of E'_∞ and of J. The fraction of rejected Monte Carlo integration points increases as R decreases as a result of more severe configurational restrictions imposed by the transitional mode potential at smaller R. In order to maintain the relative accuracy at $\lesssim 1.5\%$ for all R values it was therefore neces-

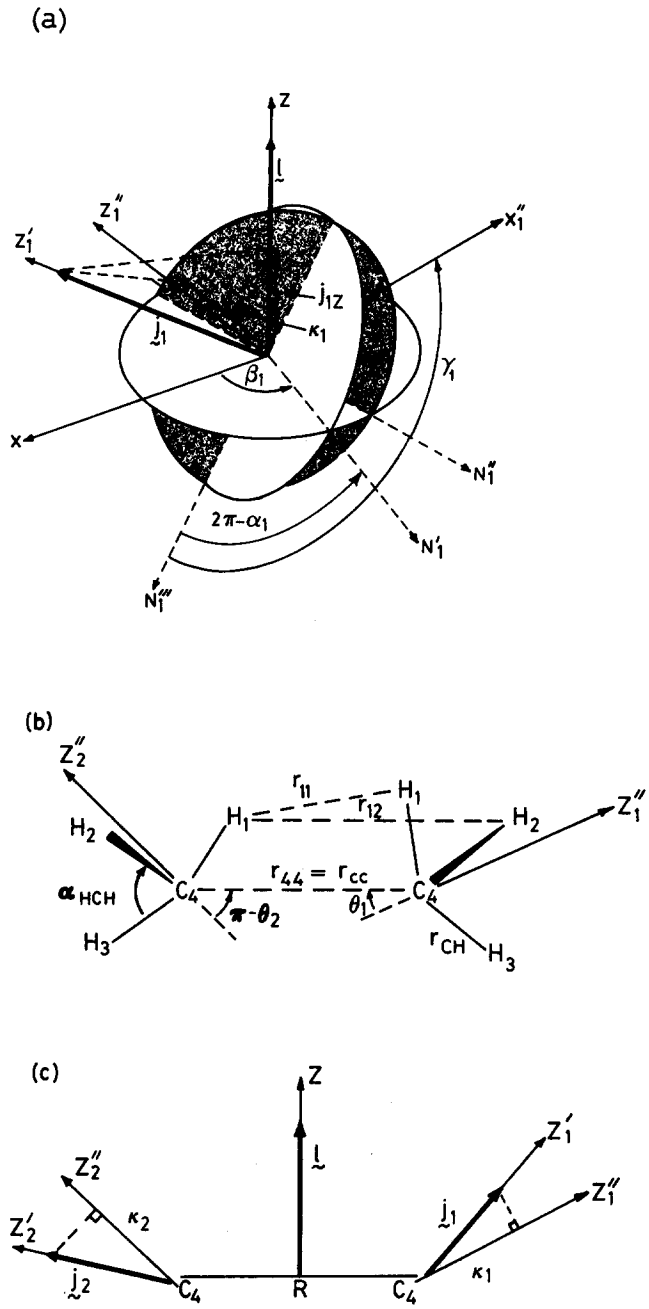

FIG. 4. (a) Euler diagram depicting the relationship between the (x, y, z), (x_1', y_1', z_1'), and (x_1'', y_1'', z_1'') Cartesian coordinate systems for the nonlinear polyatomic fragment 1. l lies along the z axis, $\mathbf{j}_1$ along the z_1' axis, and κ_1 is the projection of $\mathbf{j}_1$ on the z'' axis. Pairs of the three xy planes intersect along the lines of nodes N_1', N_1'', and N_1''', whose orientations are determined by the vectors $\mathbf{l}\times\mathbf{j}_1$, $\mathbf{l}\times\kappa_1$, and $\kappa_1\times\mathbf{j}_1$, respectively; N_1''' also serves as the x_1' axis. The angles $(\alpha_1, \theta_{l1}, \beta_1)$ are the Euler angles specifiying the orientation of the primed system relative to the unprimed system and the angles $(\gamma_1, \theta_{\kappa 1}, 0)$ are those specifying the orientation of the primed system relative to the doubly primed system. For pictorial clarity, the angle θ_{l1} between the z axis and the z_1' axis and the angle $\theta_{\kappa 1}$ between the z_1' axis and the z_1'' axis are not shown. (b) The CH bond length r_{CH}, the angle between adjacent CH bonds α_{HCH}, the bond dissociation coordinate $r_{CC} = r_{44}$, several interfragment atomic separation coordinates r_{ij}, and the angles θ_i between r_{CC} and the symmetry axis z_i'' of fragment i $(i = 1, 2)$ for the $C_2H_6 \rightarrow 2\ CH_3$ system. The carbon atom of fragment 2 is taken as the origin of $\mathbf{r}_{CC}$. (c) Angular momenta for fragment rotations and for the orbital motion of $H_3C\cdots CH_3$, the distance R between the centers of mass, and the projection κ_i of $\mathbf{j}_i$ on the z_i'' axis.

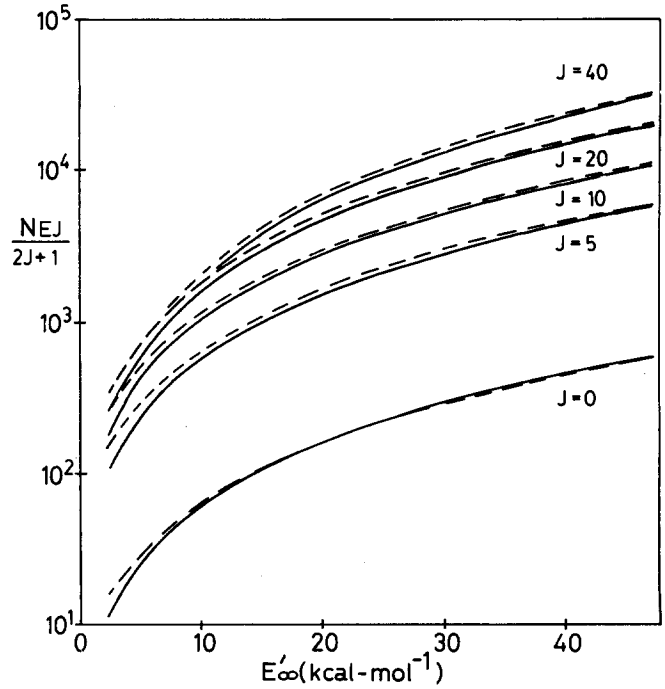

FIG. 5. Semilog plot of $N_{EJ}/(2J+1)$ vs E'_∞ in units of kcal mol^{-1} for various values of the total angular momentum J for $NO_2 \rightarrow NO + O$. E'_∞ is the energy available to the system at $R = \infty$. The solid curves depict the present results and the dashed curves are obtained from a statistical adiabatic-channel model (SACM) calculation. The statistical uncertainty in the N_{EJ} at $R^\dagger$ values resulting from the Monte Carlo calculation is too small to be resolved on the scale of the figure and has been omitted.

sary to increase the absolute number of points smoothly from 3000 in the region of zero potential ($R = \infty$) to 35 000 at $R = 1.9$ Å, the smallest separation considered.

The present method can be used with any potential energy surface, *ab initio* or semiempirical. However, for purposes of this paper the potential energy function (Appendix A) used was designed so as to facilitate a comparison with statistical adiabatic channel model (SACM)[19] calculations. In the latter, outlined in Appendix H, vibrationally adiabatic channel curves are constructed by assuming that a universal interpolating function[19] smoothly connects reactant and product eigenvalues. The surface specified in Appendix A leads to molecular parameters which would approximately yield this interpolation formula. The SACM calculated results are also given in Fig. 5 as a function of energy for various J's.

To determine the extent of looseness of the transition state, the value of $N_{EJ}(R^\dagger)$ was compared with the value at $R = \infty$, $N_{EJ}(\infty)$, for various E's and J's. For J's of 0, 20, and 40, the ratio $N_{EJ}(R^\dagger)/N_{EJ}(\infty)$ varied over the intervals (0.53 to 0.89), (0.48 to 0.86), and (0.36 to 0.81), respectively, when E'_∞ was varied from 2.29 to 47.29 kcal mol^{-1}.

B. Dependence of N_{EJ} on the potential energy function

In the absence of accurate theoretical calculations for the interfragment potentials in the region of separation distances of interest—frequently two to five times the equilibrium bond length for simple bond-fission reactions—it is common to use a Morse function to model the bond-fission part

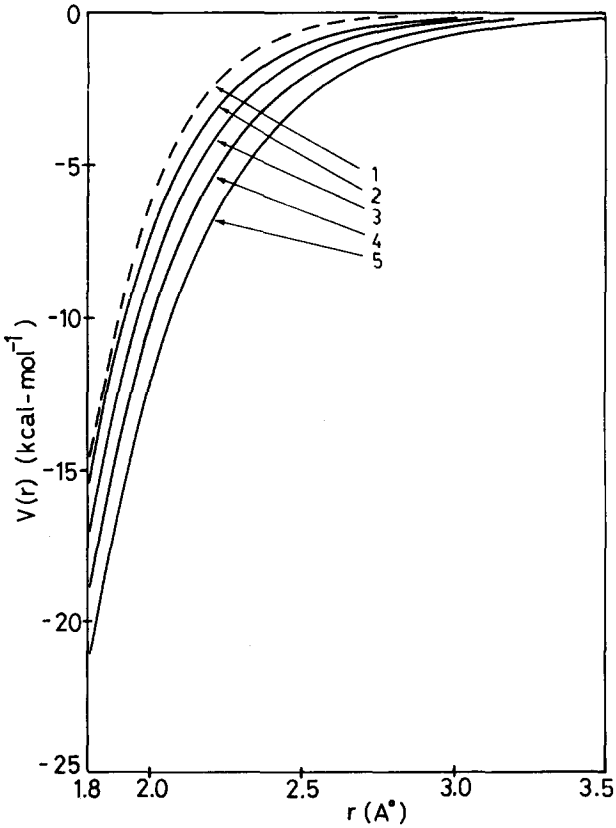

FIG. 6. The various bond dissociation potential energy curves used in the model potential energy surface for the $NO_2 \rightarrow NO + O$ system are depicted. Only the range 1.8–3.5 Å is shown and $V = 0$ corresponds to separated fragments. Curve 1 is a Varshni potential, curve 4 a Morse function, and curves 2, 3, and 5 are Morse functions modified by altering β as described in the text.

of the potential energy function V_t in Eq. (5).[19,20] However, for many diatomic molecules the Morse function is often inaccurate at larger separation distances, usually being lower than the experimentally based RKR potential curve and rising less steeply as the bond length is increased.[19,21] Accordingly, the sensitivity of N_{EJ} to modifications of the bond-fission potential V_{bf} was examined next.

One approach to obtaining improved potential curves is to let the Morse parameter β depend on the bond length or reaction coordinate.[22] For simplicity, $\beta(R)$ now has the form

$$\beta(R) = \beta_\infty + (\beta_M - \beta_\infty) g(R), \tag{11}$$

where $g(R)$ is an interpolation function, β_M is the Morse value for the ON–O bond (given later in Table A1), and β_∞ is chosen to have several different values. The function $g(R)$ was chosen to be that given in Eq. (A2). The potential energy curves labeled 2, 3, 4, and 5 in Fig. 6 correspond to choices of β_∞ such that the value of $\beta(R)$ at $R = (R_e + 3$ Å$)$ equals β_M multiplied by a factor of 1.2, 1.1, 1.0, and 0.9, respectively. Also plotted in Fig. 6 (curve 1) is a Varshni potential for the ON–O stretch.[23] The latter is similar to the above modified Morse curve with the multiplication factor equal to 1.3. In Table IV Monte Carlo estimates, $(N_{EJ}^{MC} \pm \sigma^{MC})/(2J+1)$, based on the above choices for $\beta(R)$, are given for N_{EJ} for a low, medium, and high energy for each of three J values. N_{EJ}^{MC} was calculated, now in R increments of 0.2 Å, to locate the transition state at $R^\dagger$. The $R^\dagger$ values corresponding to the entries in Table IV are given in Table V.

While an interpolation function $g(q) = \exp[-\alpha(q - q_e)]$, where q is the reaction coordinate, has been assumed in the SACM treatment,[19] and also elsewhere to approximate transitional bending frequencies in a RRKM-type model,[20] recent *ab initio* calculations[21] on the $CH_4 \rightarrow CH_3 + H$ potential energy surface and subsequent analytical fitting[24] suggested an inadequacy of this interpolation for describing the quadratic force constant for a bending motion involving the angle between a C–H bond in CH_3 and C–H interfragment displacement vector. The sensitivity of the value of $N_{EJ}(R^\dagger)$ to the form of the bending potential V_{bend} for $NO_2 \rightarrow NO + O$ was tested next. In particular, the g^2 in Eq. (A4) for V_{bend} was replaced by $\frac{1}{3}(2g + g^2)$, an interpolation reported to reproduce satisfactorily R-dependent eigenvalues for a particular 1D hindered rotor potential.[25] In Fig. 7 the values of g, g^2, and $\frac{1}{3}(2g + g^2)$ are plotted vs $(R - R_e)$ for $\alpha = 1.3$ Å^{-1}. The values of $[N_{EJ}^{MC}(R^\dagger) \pm \sigma^{MC}]/(2J+1)$ and $R^\dagger$ for the two interpolations used for V_{bend}, g^2, and $\frac{1}{3}(2g + g^2)$ are compared in Table VI.

TABLE IV. Dependence of $N_{EJ}(R^\dagger)$ on V_{bf} for $NO_2 \rightarrow NO + O$.[a]

J ($\hbar = 1$)	$E'_\infty - 2.29$ (kcal mol^{-1})	$[N_{EJ}^{MC}(R^\dagger) \pm \sigma^{MC}]/(2J+1)$ 1	2	3	4	5
0	0	8.5 ± 0.1	9.7 ± 0.1	10.7 ± 0.1	11.8 ± 0.1	13.8 ± 0.2
	20	160 ± 1	167 ± 1	178 ± 1	191 ± 1	203 ± 1
	40	457 ± 1	469 ± 2	484 ± 2	504 ± 2	526 ± 1
10	0	124 ± 2	141 ± 2	154 ± 2	175 ± 2	206 ± 3
	20	2730 ± 20	2860 ± 20	3060 ± 20	3310 ± 20	3540 ± 20
	40	8220 ± 30	8420 ± 30	8700 ± 40	8960 ± 40	9490 ± 40
20	0	139 ± 2	163 ± 3	187 ± 3	229 ± 3	283 ± 3
	20	4580 ± 30	48100 ± 40	5150 ± 40	5600 ± 40	6050 ± 30
	40	14600 ± 100	15000 ± 100	15500 ± 100	16100 ± 100	16900 ± 100

[a] The columns labeled 1–5 refer to the use of the similarly numbered potential energy curves in Fig. 6 for the bond-fission potential V_{bf}.

TABLE V. Dependence of $R^\dagger$ on V_{bf} for $NO_2 \rightarrow NO + O$.[a]

J ($\hbar = 1$)	$E'_\infty - 2.29$ (kcal mol^{-1})	$R^\dagger$(Å) 1	2	3	4	5
0	0	2.8	2.9	3.0	3.0	3.0
	20	2.4	2.4	2.4	2.5	2.6
	40	2.4	2.4	2.4	2.5	2.5
10	0	2.9	3.0	3.0	3.0	3.0
	20	2.4	2.4	2.4	2.5	2.6
	40	2.4	2.4	2.4	2.4	2.4
20	0	3.0	3.0	3.0	3.0	3.1
	20	2.4	2.4	2.4	2.5	2.6
	40	2.3	2.3	2.3	2.4	2.4

[a]The columns labeled 1–5 are defined in Table IV, Footnote a.

V. SPECIFIC RATE CONSTANTS FOR ETHANE DECOMPOSITION

To assess further the practicality of the present method, microcanonical decomposition rate constants k_{EJ} [Eq. (1)] for $C_2H_6 \rightarrow 2CH_3$ were calculated as a function of energy for several J values. The numerator $N_{EJ}(R^\dagger)$ in Eq. (1) was taken to be minimum in $N_{EJ}(R)$ on an equally spaced set of R values with $\Delta R = 0.1$ Å. The $N_{EJ}(R)$ values were obtained from Eq. (E8) and the methods described in Sec. III and Appendix F. Further details, including $R^\dagger$ values and an energy, and R-dependent restriction on the realtive orientation of the two methyl radicals, are given in Ref. 7. To obtain a simple yet realistic estimate of the density of states ρ_{EJ} in Eq. (1) a straightforward approach was adopted, yielding[26]

$$\rho_{EJ} = (2J+1)\rho_v(E'_r - J^2/2I_{A,r})F_\rho(E'_r,J)\sigma_r^{-1}, \qquad (12)$$

where σ_r is the symmetry number for the reactant. In Eq. (12) the total energy available to the reactant E'_r is E'_∞ plus the dissociation energy into the two methyl groups D_0(C–C), $I_{A,r}$ is the moment of inertia perpendicular to the symmetry axis of C_2H_6 with its equilibrium geometry, and $F_\rho(E'_r,J)$ is a rotational correction factor given in Appendix I. For harmonic oscillators the density of vibrational states ρ_v is given, in the Whitten–Rabinovitch approximation,[27] by

$$\rho_v(x) = [x + a(x)E_{Zr}]^{s-1} \Big/ \left[\Gamma(s)\prod_{i=1}^{s} h\nu_i\right], \qquad (13)$$

where $x = E'_r - J^2/2I_{A,r}$, ν_i is the frequency of the ith normal mode of C_2H_6 (Tables IX and X), E_{Zr} is the zero point energy of the reactant, and s is the number of its oscillators. For ethane $s = 18$ when the torsional motion of the CH_3 groups is treated as a vibration, as we shall do, for convenience in the present illustrative calculations. The parameter $a(x)$ is a function defined by Whitten and Rabinovitch.[27(b)]

The rate constant expression is

$$k_{EJ} = N_{EJ}(R^\dagger)/h\,(2J+1)\rho_v(x)F_\rho(x,J)\sigma_r^{-1}. \qquad (14)$$

For the present model of the reactant molecule, $\sigma_r = 6$. As discussed in Appendix E a value of $\sigma = 72$ is used in the expression for N_{EJ} [Eq. (E8)] for the case of nearly loose transition states. Results for k_{EJ} vs E'_∞ for a wide range of J values are shown in Fig. 8. For each J the energy ranges from near threshold to $E'_\infty \cong 63$ kcal mol^{-1}.

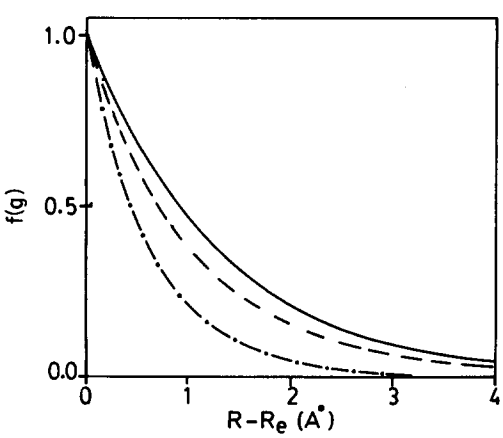

FIG. 7. Interpolation functions $f(g)$ used to construct model potential energy surfaces for the $NO_2 \rightarrow NO + O$ system. Plotted vs $(R - R_e)$ are $g = \exp[-\alpha(R - R_e)]$ (—), $\frac{1}{3}[2g + g^2]$ (– –), and g^2 (—·—). Here, $\alpha = 1.3$ Å^{-1} and R_e is the equilibrium value of R for NO_2.

VI. DISCUSSION

A. $NO_2 \rightarrow NO + O$

The values of $N_{EJ}(R^\dagger)$ calculated by the present method were seen in Sec. IV to be close to those at $R = \infty$, $N_{EJ}(\infty)$. Thus, the transition state for the model potential is relatively loose. The values were also close to those calculated in Ref. 19, as is seen from Fig. 5, except at low energies, where small differences in the molecular properties of the surface would have the largest effect. Our experience was that the present method was computationally faster than SACM at $J = 20$ and 40, even for a molecular system as small as $NO_2 \rightarrow NO + O$, presumably because of the large number of reactant and product states which occur at these J's and E'_∞'s. (The most probable thermal value of J for NO_2 at 500 K is about 40.)

The dependence of $N_{EJ}/(2J+1)$ on V_{bf} is seen from Table IV to be relatively minor for the range of energies, J's and functions considered, particularly at $E'_\infty = 42.29$ kcal

TABLE VI. Dependence of $N_{EJ}(R^\dagger)$ and $R^\dagger$ on V_{bend} for $NO_2 \rightarrow NO + O$.

J ($\hbar = 1$)	$E'_\infty - 2.29$ (kcal mol^{-1})	$[N_{EJ}(R^\dagger) \pm \sigma^{MC}]/(2J+1)$ g^2	$\frac{1}{3}[2g + g^2]$	$R^\dagger$(Å) g^2	$\frac{1}{3}[2g + g^2]$
0	0	11.8 ± 0.1	5.7 ± 0.1	3.0	3.2
	20	191 ± 1	115 ± 1	2.5	2.6
	40	504 ± 2	354 ± 2	2.4	2.4
10	0	175 ± 2	89 ± 2	3.0	3.3
	20	3310 ± 20	1960 ± 20	2.5	2.6
	40	8960 ± 40	6370 ± 40	2.4	2.4
20	0	229 ± 3	98 ± 3	3.0	3.4
	20	5600 ± 40	3410 ± 30	2.5	2.7
	40	16100 ± 100	11100 ± 100	2.4	2.4

mol^{-1}. Such results are not unexpected. Because of the looseness of the transition state, the value of N_{EJ} is relatively insensitive to V_{bf}. A significantly stronger dependence of the rate on V_{bf} has been reported for a different bond-fission system.[28]

For all J values in Table VI the N_{EJ} values calculated from g^2 exceed those calculated from $\frac{1}{3}(2g + g^2)$ by a factor of roughly 2, a result understood by comparing the two forms of V_{bend} in Fig. 7: The larger bending force frequency arising in the $\frac{1}{3}(2g + g^2)$ interpolation yields a smaller $\Omega_J(\epsilon)$ and hence a smaller value for N_{EJ}.

B. $C_2H_6 \rightarrow 2CH_3$

Since detailed results for this reaction will be given elsewhere and compared with experimental values as well as with other calculations,[7] only several remarks are made here: It can be seen from Fig. 8 that the effective threshold energy increases with J, as expected from the centrifugal effect and in agreement with other work.[26(a),41] (Actual determination of a threshold energy would require a quantum treatment for the zero point energy of the transition modes, a not too difficult task.) The energy dependence of the k_{EJ} curves in Fig. 8 is at least in qualitative agreement with that obtained elsewhere[26(a)] for a different model of the $C_2H_6 \rightarrow 2CH_3$ system.

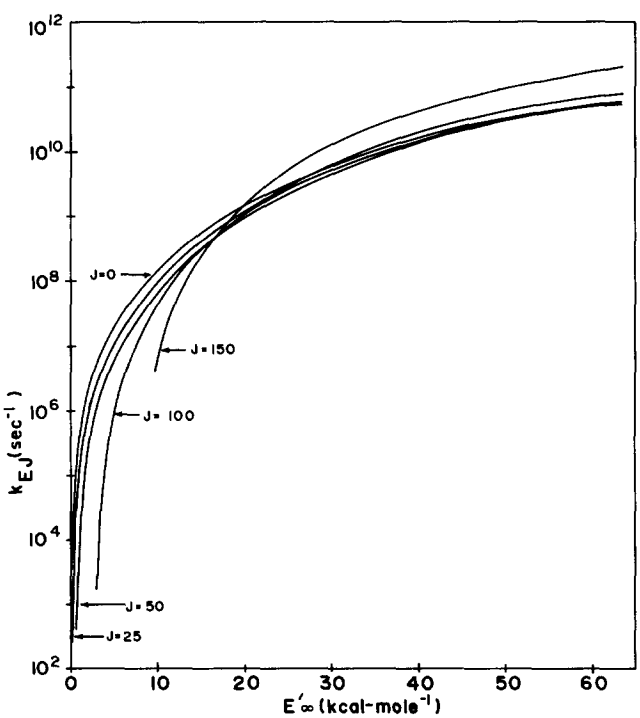

FIG. 8. Semilog plot of specific rate constants k_{EJ} vs E'_∞ for various values of J for the $C_2H_6 \rightarrow 2\ CH_3$ reaction. The statistical uncertainty in the k_{EJ} values resulting from the Monte Carlo evaluation of N_{EJ} is, in general, too small to be resolved on the scale of the figure and has been omitted.

C. Quantum correction for transitional modes

The present method provides a practical method for calculating k_{EJ}'s for arbitrary potential energy surfaces. However, it can be anticipated that sufficiently near the threshold energy a quantum correction for the transitional modes will be necessary, particularly when the contribution of the cumulative density of states of those modes $\int_0^\epsilon \Omega_J(x)dx/(2J+1)$ for a typical ϵ in Eq. (9) is comparable with unity. (There must be at least one quantum state in these transitional modes.) For the calculations in the present paper, this quantity always exceeded unity by an appreciable amount. We are currently extending the theory in this direction. A simple form of correction is the following: the value of N_{EJ} in Eq. (2) when ϵ equals the zero point energy ϵ_0 of the transitional modes is usually $(2J+1)N_V(E' - \epsilon_0)$. This value can be connected by interpolation to values of N_{EJ} given by Eq. (2) at somewhat higher energies. This correction would, by placing a lower limit on N_{EJ}, prevent the expression in Eq. (2) from becoming too small, i.e., less than $(2J+1)$, when E' becomes small enough that the system as a whole is in its ground state for the given value of the reaction coordinate.

VII. CONCLUSIONS

The above results show that the present method can be used to treat in a practical way unimolecular dissociations having transition states of arbitrary looseness. The dependence of results for the $NO_2 \rightarrow NO + O$ reaction on the potential energy function for bond fission and for bending was examined for a given set of model surfaces, with results given in Tables IV–VI. The present method can be used, however, with any potential energy surface. When a particular surface was chosen which led to molecular parameters having an

interpolation between those of reactants (NO_2) and products (NO + O) analogous to the universal eigenvalue interpolation assumed in the SACM model, fairly similar results were obtained. The main attributes of the present method are its use of general potential energy functions and a computational feasibility which is unaffected by the size of the polyatomic fragments.

ACKNOWLEDGMENTS

It is a pleasure to acknowledge the support of this research by the National Science Foundation, USA, and (DMW) by a NSERC of Canada Postdoctoral Research Fellowship.

APPENDIX A: POTENTIAL ENERGY PARAMETERS AND COORDINATE TRANSFORMATION FOR $NO_2 \rightarrow NO + O$

For the reaction $NO_2 \rightarrow NO + O$ a model potential $V = V_c + V_t$ was used, where V_c denotes the NO bond potential (coordinate r) and V_t denotes the contribution to V arising from the angular coordinates and the ON–O separation distance [Eq. (A3)]. V_c is taken to be a Morse potential function of r:

$$V_c \equiv V_c(r;R) = D(R)(1 - \exp\{-\beta(R)[r - r_e(R)]\})^2 - D(R), \quad \text{(A1)}$$

whose parameters D, β, and r_e themselves depend on R, the separation distance between the centers of mass of the two fragments. $D(R)$ is a bond dissociation energy, $\beta(R)$ a Morse parameter, and $r_e(R)$ an equilibrium bond length at any given R.

Denoting D, β, and r_e^{-2} by $X(R)$, an interpolation was used for these quantities,

$$X(R) = X_{\text{O-N}} - (X_{\text{O-N}} - X_{\text{ON-O}})g(R),$$

$$g(R) = \exp[-\alpha(R - R_e)], \quad \text{(A2)}$$

where R_e is the value of R at the equilibrium geometry of NO_2. The subscripts ON–O and O–N indicate reactant and product quantities, respectively, for the NO bond. The form of the interpolation function $g(R)$ is that proposed in Ref. 19. It was chosen here mainly to facilitate a comparison of the calculated N_{EJ} with the value for the statistical adiabatic-channel model of Ref. 19. However, in Ref. 19 a potential surface was not used but rather frequencies, moments of inertia, and angular momenta interpolated by $g(R)$.

The transitional-mode potential V_t was taken to be

$$V_t = V_{\text{bf}}(r_{\text{ON-O}}) + V_{\text{bend}}(\theta), \quad \text{(A3)}$$

where the bond-fission potential V_{bf} is a Morse function, as in Eq. (A1) but with r replaced by $r_{\text{ON-O}}$ and with D, β, and r_e being constants, namely the values for ON–O. The bending potential was modeled with a hindered rotor function,

$$V_{\text{bend}} = \tfrac{1}{2} f_\theta g^2(R) \sin^2(\theta - \theta_e), \quad \text{(A4)}$$

where f_θ is a quadratic bending force constant and θ_e is the equilibrium value of θ in NO_2. The $g^2(R)$ factor makes the bending vibration frequency vary as $g(R)$. The various coordinates used in Eqs. (A1)–(A4) are depicted in Fig. 1 and the relevant potential parameters are listed in Table A1.

In the text the internal coordinates were first converted to Jacobi coordinates and then the latter were expressed in terms of action-angle variables. The first transformation is made as follows: The three atoms lie in a plane, regarded as the body-fixed xy plane, and with an origin at the center of mass of the AB molecule. The coordinates are given in terms of r and γ: $x_A = (\mu/m_A) r \cos\gamma$, $y_A = (\mu/m_A) r \sin\gamma$, $x_B = -(\mu/m_B) r \cos\gamma$, $y_B = -(\mu/m_B) r \cos\gamma$, $x_C = R$, $y_C = 0$. The BC bond distance, $r_{\text{AB-C}}$, and the ABC bond angle θ are readily expressed in terms of these coordinates.

TABLE A1. Potential parameters for NO_2 system.

Parameter	Value	Reference	Parameter	Value	Reference
		NO_2			
$r_{\text{ON-O},e}$	1.1934 Å	30	R_e	1.699 Å	a
θ_e	134.07°	30	$D_{\text{ON-O}}$	74.5 kcal mol^{-1}	b
ν_1	1356.9 cm^{-1}	30	$\beta_{\text{ON-O}}$	3.266 Å^{-1}	c
ν_2	754.1 cm^{-1}	30	f_θ	1.579×10^{-11} erg	d
ν_3	1665.6 cm^{-1}	30	I_{Ae}	2.10 amu Å^2	a
f_{rr}	11.04×10^5 erg cm^{-2}	30	I_{Be}	38.62 amu Å^2	a
f_{aa}	1.109×10^5 erg cm^{-2}	30	I_{Ce}	40.73 amu Å^2	a
D_0(ON–O)	3.114 eV	31			
		NO			
$r_{\text{NO},e}$	1.1508 Å	32	D_{ON}	152.6 kcal mol^{-1}	b
ν	1903.6 cm^{-1}	32	β_{ON}[e]	2.742 Å^{-1}	c
D_0(NO)	6.5 eV	32			
α	1.3 Å^{-1}	19[f]			

[a] Determined by $r_{\text{ON-O},e}$ and atomic masses.
[b] $D_{\text{ON-O}} = D_0(\text{ON–O}) + E_{zr} - E_{zp}$ and $D_{\text{ON}} = D_0(\text{ON}) + E_{zp}$; $E_{zr} = (2\pi/2)(\nu_1 + \nu_2 + \nu_3)$ and $E_{zp} = (2\pi/2)\nu$ (in units of $\hbar = 1$).
[c] $\beta_{\text{ON-O}} = [f_{rr}/2D_{\text{ON-O}}]^{1/2}$, where f_{rr} is the diagonal quadratic stretching force constant for NO_2.
[d] $f_\theta \equiv f_{aa}[r_{\text{ON-O},e}]^2$ where f_{aa} is the diagonal quadratic bending force constant for NO_2.
[e] $\beta_{\text{ON}} = 2\pi\nu[\mu/2D_{\text{ON}}]^{1/2}$.
[f] This value was found to provide a good fit of the statistical adiabatic-channel model to high-pressure thermal rate constant data (Ref. 19).

APPENDIX B: POTENTIAL ENERGY PARAMETERS FOR $H_2O_2 \rightarrow 2OH$

For the reaction $H_2O_2 \rightarrow 2OH$ a model potential $V = V_{c1} + V_{c2} + V_t$ analogous to that described in Appendix A was used. Each V_{ci} denotes an OH bond potential with coordinate $r_i (i = 1, 2)$, similar to Eq. (A1) with r now replaced by r_i. Denoting D, β, and r_e^{-2} by $X(R)$, the interpolation used was again given by Eq. (A2), with ON–O and O–N subscripts replaced by HOO–H and O–H to indicate the values for the OH bond in the reactant and separated products, respectively. The transitional mode potential V_t was modeled by

$$V_t = V_{bf}(r_{HO\text{-}OH}) + V_{b1}(\theta_1) + V_{b2}(\theta_2) + V_\tau(\tau,\theta_1,\theta_2). \tag{B1}$$

The bond-fission potential V_{bf} was again taken to be a Morse function, as in Eq. (A1), with r, D, β, and r_e being the values for HO–OH, the latter three now being constants. The bending potentials $V_{bi} (i = 1, 2)$ were chosen to be hindered rotor functions similar to that in Eq. (A4), but now with i subscripts added to the θ's and with $\theta_{i,e}$ being the equilibrium H–O–O bond angle in H_2O_2 $(i = 1, 2)$. The torsional potential V_τ in Eq. (B1) is a hindered rotor function, modified by coupling to the bending modes. It is typically small in the coordinate domain of interest:

$$V_\tau = [V_0 + V_1 \cos \Delta\tau + V_2 \cos 2\Delta\tau + V_3 \cos 3\Delta\tau] \times \sin\theta_1 \sin\theta_2\, g(R), \tag{B2}$$

where $\Delta\tau = \tau - \tau_e$ and τ_e is the equilibrium value of the torsional angle τ in H_2O_2. The $\sin\theta_1 \sin\theta_2$ factor varies between 0 and 1, since $0 \leqslant \theta_i \leqslant \pi$, and ensures that the torsional potential is physically reasonable when θ_i tends to 0 or π. The change in the equilibrium properties of H_2O_2 introduced by this factor proved to be minor since $\theta_{1,e}$ and $\theta_{2,e}$ are close to $\pi/2$ for H_2O_2. The $g(R)$ interpolation used in Eq. (B2) for the torsional potential, namely that given by Eq. (A2), is somewhat similar to that used in Ref. 33 for a 1D hindered rotation about a threefold symmetry axis. The various coordinates used in the above equations are depicted in Fig. 3. The relevant potential parameters are listed in Table B1.

APPENDIX C: POTENTIAL ENERGY PARAMETERS FOR $C_2H_6 \rightarrow 2CH_3$

For this larger system a model potential $V = V_c + V_t$ was used, where V_t, the potential energy function for variation of the separation distance and orientation of the CH_3

TABLE B1. Potential parameters for H_2O_2 system.

Parameter	Value	Reference	Parameter	Value	Reference
		H_2O_2			
$r_{HOO\text{-}H,e}$	0.965 Å	34	R_e	1.485 Å	b
$r_{HO\text{-}OH,e}$	1.462 Å	34	$D_{HO\text{-}OH}$	54.6 kcal mol^{-1}	c
$\theta_{1,e}, \theta_{2,e}$	100°	34	$D_{HOO\text{-}H}$	95.8 kcal mol^{-1}	c
τ_e	120°	34	$\beta_{HO\text{-}OH}$	2.388 Å^{-1}	d
ν_1	3599 cm^{-1}	35	$\beta_{HOO\text{-}H}$	2.453 Å^{-1}	d
ν_2	1402 cm^{-1}	35	$f_{\theta_1}, f_{\theta_2}$	1.26×10^{-11} erg	e
ν_3	877 cm^{-1}	35	V_0	876.3 cm^{-1}	38[f]
ν_4	243 cm^{-1}	35	V_1	1093.4 cm^{-1}	38[f]
ν_5	3608 cm^{-1}	35	V_2	546.7 cm^{-1}	38[f]
ν_6	1266 cm^{-1}	35	V_3	−56.4 cm^{-1}	38[f]
f_{RR}	4.322×10^5 erg cm^{-2}	36[a]			
f_{rr}	8.009×10^5 erg cm^{-2}	36[a]			
f_{aa}	0.894×10^5 erg cm^{-2}	36[a]			
D_0(HO–OH)	49.5 kcal mol^{-1}	37			
D_0(HOO–H)	88.5 kcal mol^{-1}	37			
		HO_2			
ν_1'	3410 cm^{-1}	39			
ν_2'	1095 cm^{-1}	39			
ν_3'	1390 cm^{-1}	39			
		OH			
$r_{OH,e}$	0.9710 Å	40	D_{OH}	105.6 kcal mol^{-1}	c
ν	3735 cm^{-1}	40	β_{OH}	2.285 Å^{-1}	g
D_0(OH)	4.35 eV	40			
α	1.0 Å^{-1}	h			

[a] The harmonic stretching force constants f_{RR} and f_{rr} for O–O and O–H, respectively, as well as the harmonic H–O–O bending force constant f_{aa} are *ab initio*/empirical values taken from Table 1 of Ref. 36.

[b] Determined by given equilibrium geometry and atomic masses of H_2O_2.

[c] $D_{HO\text{-}OH} = D_0(\text{HO–OH}) + E_{zr} - 2E_{zp}$; $D_{HOO\text{-}H} = D_0(\text{HOO–H}) + E_{zr} - E_z'$; $D_{OH} = D_0(\text{OH}) + E_{zp}$; where (with $\hbar = 1$) $E_{zr} = (2\pi/2)\sum_{i=1}^{6} \nu_i$, $E_z' = (2\pi/2)\sum_{i=1}^{3} \nu_i'$, and $E_{zp} = (2\pi/2)\nu$.

[d] $\beta_{HO\text{-}OH} = [f_{RR}/2D_{HO\text{-}OH}]^{1/2}$, $\beta_{HOO\text{-}H} = [f_{rr}/2D_{HOO\text{-}H}]^{1/2}$.

[e] $f_{\theta_i} = f_{aa}[r_{HOO\text{-}H,e}][r_{HO\text{-}OH,e}] (i = 1, 2)$.

[f] Our values of V_0, V_1, V_2, V_3 are determined by the experimental barrier heights reported in Ref. 38 and by requiring $V_\tau(0) = \partial V_\tau(0)/\partial\tau = 0$.

[g] $\beta_{OH} = 2\pi\nu(\mu_{OH}/2D_{OH})^{1/2}$.

[h] In Ref. 19, α was obtained by fitting to thermal rate constant data. In the absence of such fits for H_2O_2, we adopt the "standard" value (Refs. 19 and 41) of $\alpha = 1.0$ Å^{-1}.

TABLE C1. Correlation of conserved vibrations.[a]

Label i	Mode	C_2H_6 Symmetry type	ν	$\bar{\nu}_{ir}$	Mode	CH_3 Symmetry type	ν_{ip}
1	ν_1	A_{1g}	2954	2925.0	ν_1	A_1'	3044
	ν_5	A_{2u}	2896				
2	ν_2	A_{1g}	1388	1383.5	ν_2	A_2''	580
	ν_6	A_{2u}	1379				
3	ν_7	E_u	2985	2977.0	ν_3	E'	3162
	ν_{10}	E_g	2969				
4	ν_8	E_u	1472	1470.5	ν_4	E'	1396
	ν_{11}	E_g	1469				

[a] All frequencies are in units of cm^{-1} and are taken from Ref. 19.

groups, is given later in Eq. (C3). The potential V_c for the "conserved" vibrational degrees of freedom (listed in Table C1) was assumed for simplicity to be separable and quadratic. Their vibrational energy in excess of the zero point energy was then expressed in terms of principal quantum numbers n_{i1} and n_{i2} of normal modes in methyl fragments 1 and 2:

$$E'_V = \sum_{i=1}^{4} 2\pi\nu_i(R)[n_{i1} + n_{i2}]. \tag{C1}$$

The sum is over the (identical) vibrations of each methyl group, two of which are doubly degenerate. The frequencies $\nu_i(R)$ were obtained by interpolation:

$$\nu_i(R) = \nu_{ip} + (\bar{\nu}_{ir} - \nu_{ip})g(R)[i = 1,...,4], \tag{C2}$$

where R is the separation distance between the centers of mass of the methyl fragments and g is given by Eq. (A2). The product frequencies ν_{ip} are the normal mode frequencies of an isolated methyl radical and are listed with their symmetry type in Table C1. The reactant's frequencies $\bar{\nu}_{ir}$, which correlate to the ν_{ip} via Eq. (C2), were determined as follows: For a given symmetry type (either A or E) and for each type of vibration (either CH_3 stretching or CH_3 deformation) two nearly degenerate frequencies were averaged. The resultant $\bar{\nu}_{ir}$'s were then correlated on a 1:1 basis with the ν_{ip}'s according to symmetry type and characteristic vibrational motion[19] and are listed in Table C1, together with their symmetry type. The remaining normal vibrational modes of C_2H_6 become transitional modes as R increases and are listed in Table C2.

The potential V_t for the "transitional" degrees of freedom and for the bond-fission coordinate r_{CC} is assumed to arise from nonbonded and bonded interactions,

$$V_t = V_{NB} + V_B, \tag{C3}$$

described below.

TABLE C2. Disappearing vibrational modes of C_2H_6.[a]

Mode	Symmetry type	ν	Description
ν_3	A_{1g}	995	C–C stretch
ν_4	A_{1u}	289	torsion
ν_9	E_u	821	CH_3 rock
ν_{12}	E_g	1206	CH_3 rock

[a] All frequencies are in cm^{-1} and are taken from Ref. 19.

1. Nonbonded interaction V_{NB}

Between all nonbonded H···H and C···H pairs a Lennard-Jones potential V_{LJ}, given by $\epsilon[(r_0/r)^{12} - 2(r_0/r)^6]$, was used and Coulomb interactions arising from residual point charges on different atoms were neglected.[42] The resultant nonbonded potential is

$$V_{NB} = \sum_{i,j=1}^{4}{}' V_{LJ}(r_{ij}), \tag{C4}$$

where i and j label atoms on different CH_3 fragments and the prime indicates that the C···C contribution is excluded. The parameters for the various V_{LJ}'s are listed in Table C3.

2. Bonded interaction V_B

For the C···C bond-fission potential a Morse function was used, modified by an orientational factor to include in an approximate way the influence of the now-bent C···C bond[43]:

$$V_B = V_M^{eff}(r_{CC})\cos^2\theta_1 \cos^2\theta_2, \tag{C5}$$

where an effective potential V_M^{eff} was introduced:

$$V_M^{eff} = D_{CC}^{eff}\{1 - \exp[-\beta_{CC}^{eff}(r_{CC} - r_{CC,e}^{eff})]\}^2 - D_{CC}^{eff}. \tag{C6}$$

Here, $r_{CC}(= |\mathbf{r}_{CC}|)$ is the carbon–carbon separation distance and θ_i is the angle between $\mathbf{r}_{CC}$ and the symmetry axis of $(CH_3)_i (i = 1, 2)$.

The effective Morse parameters in Eq. (C6) were determined by a least-squares fit of a known C–C Morse function V_M to the sum of the potentials $V_{NB} + V_B$ given by Eqs. (C3) to (C6) and evaluated along the minimum energy path from reactant to products. The latter was obtained by constraining the CH_3 groups to be in the same relative orientation as in equilibrium $C_2H_6[\theta_1 = 0, \theta_2 = \pi$ in Eq. (C5)] and by using the interpolated R-dependent CH_3 structure described below. A least-squares fit over the r_{CC} interval of 1.75 to 6.78 Å yielded a V_M^{eff} with a root-mean-square deviation of 0.35 kcal mol^{-1} from V_M. The largest deviations occurred in the 1.75 to 2.1 Å interval, a region for which the potential was not needed. In the region of particular interest, namely, $r_{CC} \gtrsim 2.2$ Å, V_M^{eff} was slightly less negative than V_M.

In order that the structure of each CH_3 group evolved smoothly when R was varied, from that in C_2H_6 to that of an isolated methyl radical, the local equilibrium carbon–hydrogen bond length r_{CH} and the H–C–H bond angle α_{HCH} were

TABLE C3. Potential parameters for C_2H_6 system.

Parameter	Value	Reference	Parameter	Value	Reference
		C_2H_6			
$r_{CH,e}$	1.111 Å	34	R_e	1.696 Å	b
$r_{CC,e}$	1.533 Å	34	D_{CC}	96.6 kcal mol^{-1}	c
$\alpha_{HCH,e}$	107.3°	34	β_{CC}	1.80 Å^{-1}	d
$\beta_{HCC,e}$	111.4°	34	D_{CC}^{eff}	202.5 kcal mol^{-1}	e
τ_e	60°	34	β_{CC}^{eff}	1.90 Å^{-1}	e
f_{CC}	4.342×10^5 erg cm^{-2}	44	$r_{CC,e}^{eff}$	1.175 Å	e
D_0(C–C)	87.60 kcal mol^{-1}	34[a]			
		CH_3			
$r_{CH,e}$	1.079 Å	31	$\alpha_{HCH,e}$	120°	31
		$CH_3\cdots CH_3$			
$\epsilon_{H\cdot\cdot H}$	0.010 kcal mol^{-1}	43	$r_{H\cdot\cdot H,O}$	3.37 Å	43
$\epsilon_{C\cdot\cdot C}$	0.095 kcal mol^{-1}	43	$r_{C\cdot\cdot C,O}$	3.88 Å	43
$\epsilon_{C\cdot\cdot H}$	0.031 kcal mol^{-1}	e	$r_{C\cdot\cdot H,O}$	3.62 Å	f
α	1.0 Å^{-1}	g			

[a] Experimental value.
[b] Determined by given equilibrium geometry and atomic masses of C_2H_6.
[c] $D_{CC} = D_0(\text{C–C}) + E_{zr} - E_{zp}$ where E_{zr} and E_{zp} are determined by the normal mode frequencies of C_2H_6 and CH_3, respectively, as listed in Tables C1 and C2.
[d] $\beta_{CC} = (f_{CC}/2D_{CC})^{1/2}$.
[e] Obtained by least squares fitting as outlined in Appendix C.
[f] $\epsilon_{C\cdot\cdot H} = (\epsilon_{H\cdot\cdot H}\epsilon_{C\cdot\cdot C})^{1/2}$; $r_{C\cdot\cdot H,O} = \frac{1}{2}(r_{H\cdot\cdot H,O} + r_{C\cdot\cdot C,O})$.
[g] The standard value (Refs. 19 and 41) of $\alpha = 1.0$ Å^{-1} is adopted. A value of $\alpha = 0.82$ Å^{-1} has been used in an earlier work (Ref. 20).

obtained at each R by an interpolation:

$$r_{CH}(R) = r^p_{CH,e} + [r^r_{CH,e} - r^p_{CH,e}]g(R),$$
$$\alpha_{HCH}(R) = \alpha^p_{HCH,e} + [\alpha^r_{HCH,e} - \alpha^p_{HCH,e}]g(R). \quad \text{(C7)}$$

Here, the superscripts p and r denote product (isolated CH_3) and reactant (C_2H_6) quantities, respectively. The CH_3 structure, and the relative separation and orientation of the two CH_3 groups together determined the interfragment atomic separations and hence the V_t in Eq. (C3). In addition, the CH_3 structure determined the three moments of inertia, $I_A(R)$, $I_B(R)$, and $I_C(R)$, used to assign a (rigid-rotor) rotational energy to each fragment.

The parameters appearing in Eqs. (C4)–(C7) as well as other relevant parameters are listed in Table C3. In Fig. 4(b) the various bond angles and bond distances that determined V_t are depicted. When the actual potential energy surface is available no interpolation function $g(R)$ is needed.

APPENDIX D: ACTION-ANGLE AND INTERNAL COORDINATES AND DENSITY OF STATES FOR NONLINEAR SYSTEMS ABCD→AB + CD, SUCH AS H_2O_2→2 OH

For these systems the canonically conjugate set of action-angle variables which specifies the space-fixed orientations and angular momenta of all four atoms is $(j_1, j_{1z}, j_2, j_{2z}, l, l_z, \alpha_1, \beta_1, \alpha_2, \beta_2, \alpha_l, \beta_l)$.[1,8,9] The variables j_1 and j_2 are the individual rotational angular momentum actions of fragments 1 and 2 (i.e., the linear species AB and CD, respectively), j_{1z} and j_{2z} are their space-fixed z components, and l and l_z are as described in Sec. II. Instead of (j_{1z}, j_{2z}, l_z) and their conjugate angles $(\beta_1, \beta_2, \beta_l)$ it is convenient to use[9] (k, J, J_z) and their angles $(\alpha_k, \alpha, \beta)$, where k is an intermediate angular momentum action associated with a vector sum $|\mathbf{j}_1 + \mathbf{j}_2|$, α_k is its conjugate angle, and (J, J_z, α, β) are as defined before. For systems described by the above variables and for any given value of J we now have

$$\Omega_J(\epsilon) = (2\pi)^{-6}\sigma^{-1}\int\cdots\int \times dJ_z\, dj_1\, dj_2\, dk\, dl\, d\alpha\, d\beta\, d\alpha_1\, d\alpha_2\, d\alpha_k\, d\alpha_l \times \Delta(J, k, l)\Delta(k, j_1, j_2)\delta(\epsilon - H_{cl}). \quad \text{(D1)}$$

The Δ functions and the integration limits are similar to those described for Eq. (4). H_{cl} is written as

$$H_{cl} = \frac{j_1^2}{2\mu_1 r_1^2} + \frac{j_2^2}{2\mu_2 r_2^2} + \frac{l^2}{2\mu R^2} + V_t(r_{AB\text{–}CD}, \theta_1, \theta_2, \tau), \quad \text{(D2)}$$

where μ_i is the reduced mass of fragment i, and μ is the reduced mass for the relative motion of the AB and CD fragments. The potential V_t is modeled to be a function of the internal coordinates $r_{AB\text{–}CD}$ (the BC distance), θ_1, θ_2, and τ depicted in Fig. 3(a) using H_2O_2 as an example. The remaining two coordinates in Fig. 3(a) describe AB and CD vibrations and so are included in $N_V(E' - \epsilon)$. The reaction coordinate R, the angular momenta j_1, j_2, and l, the angles γ_i between $\mathbf{R}$ and $\mathbf{r}_i$ ($i = 1, 2$), and the angle λ between $\mathbf{r}_1\times\mathbf{R}$ and $\mathbf{r}_2\times\mathbf{R}$ are depicted in Fig. 3(b). V_t is described in Appendix B.

To evaluate the V_t in Eq. (D2), the internal coordinates $r_{AB\text{–}CD}$, θ_1, θ_2, and τ are first expressed in terms of the Jacobi

coordinates (R, r_1, r_2, γ_1, γ_2, λ), as in the final paragraph of this Appendix. For any R the values of r_1 and r_2 are then replaced by R-dependent equilibrium values r_e (Appendix B). The angles λ, γ_1, and γ_2 are next written as functions of J, j_1, j_2, k, l, α_1, α_2, α_k, and α_l, with the aid of the following expressions obtained from Eq. (7), with **a**, **b**, **c**, and **d** identified in Table III:

$$\cos\varphi = \cos\gamma_1 \cos\gamma_2 + \sin\gamma_1 \sin\gamma_2 \cos\lambda, \tag{D3}$$

$$\cos\gamma_i = (\cos\theta_R \cos\theta_{ri} + \sin\alpha_i \sin\alpha_l \cos\theta_{li})/\cos\alpha_k, \tag{D4}$$

where

$$\cos\varphi = \cos\alpha_1 \cos\alpha_2 + \sin\alpha_1 \sin\alpha_2 \cos\theta_{12}, \tag{D5}$$

$$\cos\theta_R = \cos\alpha_k \cos\alpha_l + \sin\alpha_k \sin\alpha_l \cos\theta_{lk}, \tag{D6}$$

and

$$\cos\theta_{ri} = \cos\alpha_k \cos\alpha_i - \sin\alpha_k \sin\alpha_i \cos\theta_{ki}. \tag{D7}$$

In these equations φ is the angle between the vectors $\mathbf{r}_1$ and $\mathbf{r}_2$, θ_R is the angle between the vectors $\mathbf{R}$ and $\mathbf{j}_1 \times \mathbf{j}_2$, and θ_{ki} is the angle between $\mathbf{l} \times \mathbf{k}$ and $\mathbf{r}_i$ ($i = 1, 2$). The cosines of various other angles in the above equations are given in terms of the desired variables in Tables I and II. H_{cl} is now seen to be completely specified by the variables (R, r_1, r_2, J, j_1, j_2, k, l, α_1, α_2, α_k, α_l) and to be independent of (J_z, α, β). Equation (D1) thus becomes

$$\Omega_J(\epsilon) = (2J+1)(2\pi)^{-4}\sigma^{-1}\int\cdots\int \times dj_1\, dj_2\, dk\, dl\, d\alpha_1\, d\alpha_2\, d\alpha_k\, d\alpha_l \times \Delta(J,k,l)\Delta(k,j_1,j_2)\delta(\epsilon - H_{cl}), \tag{D8}$$

which, combined with Eq. (2), yields the analog of Eq. (9),

$$N_{EJ} = (2J+1)(2\pi)^{-4}\sigma^{-1}\int\cdots\int \times dj_1\, dj_2\, dk\, dl\, d\alpha_1\, d\alpha_2\, d\alpha_k\, d\alpha_l \times N_V(E' - H_{cl})\Delta(J,k,l)\Delta(k,j_1,j_2). \tag{D9}$$

The evaluation of the integral in Eq. (D9) is described in Sec. III. For the particular case of H_2O_2, σ is 2. (In the case of the calculations of N_{EJ} in part I for H_2O_2 only the integral was given and not the σ^{-1} contribution.)

The coordinate transformation referred to earlier from internal to Jacobi coordinates is readily made. The AB fragment is chosen to lie in the body-fixed xy plane and the center of mass of CD to lie on the positive x axis. The coordinates of the various atoms then are as follows:

$$\begin{aligned}
x_A &= (\mu_{AB}/m_A) r_1 \cos\gamma_1,\\
y_A &= (\mu_{AB}/m_A) r_1 \sin\gamma_1,\\
z_A &= z_B = 0,\\
x_B &= -(\mu_{AB}/m_B) r_1 \cos\gamma_1,\\
y_B &= -(\mu_{AB}/m_B) r_1 \sin\gamma_1,\\
x_C &= -(\mu_{CD}/m_C) r^2 \cos\gamma_2 + R,\\
y_C &= -(\mu_{CD}/m_C) r^2 \sin\gamma_2 \cos\lambda + R,\\
z_C &= -(\mu_{CD}/m_C) r_2 \sin\gamma_2 \sin\lambda + R,\\
x_D &= (\mu_{CD}/m_D) r_2 \cos\gamma_2 + R,\\
y_D &= (\mu_{CD}/m_D) r_2 \sin\gamma_2 \cos\lambda + R,\\
z_D &= (\mu_{CD}/m_D) r_2 \sin\gamma_2 \sin\lambda + R,
\end{aligned}$$

where μ_{AB} is the reduced mass of A and B. The internal coordinates for the transitional modes, namely the BC bond length, $r_{AB\text{-}CD}$, the bond angles θ_1, θ_2, and τ are readily expressed in terms of these coordinates, e.g., $\cos\theta_i = \mathbf{e}_i \cdot \mathbf{e}_{AB\text{-}CD}$ and $\cos\tau = (\mathbf{e}_1 \times \mathbf{e}_{AB\text{-}CD}) \cdot (\mathbf{e}_2 \times \mathbf{e}_{AB\text{-}CD})/\sin\theta_1 \sin\theta_2$, where $\mathbf{e}_i$ and $\mathbf{e}_{AB\text{-}CD}$ denote unit vectors along $\mathbf{r}_i$ and $\mathbf{r}_{AB\text{-}CD}$, respectively.

APPENDIX E: ACTION-ANGLE COORDINATES, INTERNAL COORDINATES, AND DENSITY OF STATES FOR DISSOCIATION INTO POLYATOMIC FRAGMENTS

The material in this Appendix is grouped into four parts: In (1) a set of action-angle variables suited to polyatomic fragments is obtained. In (2) the density of transitional states $\Omega_J(\epsilon)$ and the classical Hamiltonian H_{cl} for the transitional modes are expressed in terms of these variables. Since the potential energy contribution to H_{cl} is modeled in this study to be a function of interfragment atomic separation distances as well as two bond angles, a transformation from the action-angle variables to these internal coordinates is given in (3). Part (4) describes the minor modifications to (2) required to treat asymmetric rather then symmetric top fragments.

1. Coordinates

For this polyatomic case, written as $X_1X_2 \rightarrow X_1 + X_2$, such as $C_2H_6 \rightarrow 2\,CH_3$, the following system of coordinates, applicable to systems with nonlinear polyatomic fragments, was introduced. We let (x, y, z) denote a set of Cartesian coordinate axes fixed in the $X_1 \cdots X_2$ system, the z axis being chosen to lie along the relative orbital angular momentum action vector $\mathbf{l}$ of the fragments, as in Fig. 4(a). The x axis is chosen to lie along a vector $\mathbf{l} \times \mathbf{k}$, where $\mathbf{k}$ is defined to be $\mathbf{j}_1 + \mathbf{j}_2$ (Appendix D). The relative separation vector $\mathbf{R}$ along the line of centers of mass of the two fragments lies in the body-fixed xy plane and is oriented at an angle α_l with respect to the x axis (α_l is conjugate to l). The vector $\mathbf{R}$ and α_l are not shown in Fig. 4(a), but are as depicted in Fig. 2, but with $\mathbf{l} \times \mathbf{j}$ then replaced by $\mathbf{l} \times \mathbf{k}$.

Two coordinate frames (x_i', y_i', z_i') and (x_i'', y_i'', z_i''), fixed in fragment X_i are defined. The doubly primed system is chosen so that the inertial tensor is diagonal in it; the z_i'' axis is the symmetry axis of X_i if the latter happens to be a symmetric top. The primed system is chosen so that the z_i' axis lies along $\mathbf{j}_i$, and the x_i' axis lies along the intersection of $x_i'\,y_i'$ and $x_i''\,y_i''$ planes, namely along N_i''' in Fig. 4(a). The projections of $\mathbf{j}_i$ on the z and z_i'' axes are denoted by j_{iz} and κ_i, respectively [Fig. 4(a)].

The angles conjugate to (j_i, j_{iz}, κ_i) are, respectively, (α_i, β_i, γ_i) as in Fig. 4(a). The z projection of l, l_z, its conjugate angle β_l, and α_l specify the orientation of the body-fixed (x, y, z) system with respect to a space-fixed system. These coordinates provide a set of variables (l, α_l, l_z, β_l, j_1, α_1, j_{1z}, β_1, κ_1, γ_1, j_2, α_2, j_{2z}, β_2, κ_2, γ_2) which specify, among other things, the orientation in space of each fragment X_i ($i = 1, 2$). Instead of (l_z, j_{1z}, j_{2z}, β_l, β_1, β_2) the variables (J, J_z, k, α, β, α_k) are used, where the symbols have the same meaning as in Appendix D. The resulting action variables are J, J_z, j_1, j_2, k, l, κ_1, κ_2 and their respective conjugate angles are α, β, α_1, α_2, α_k, α_l, γ_1, γ_2. Such action variables have been used previous-

ly for symmetric tops in statistical phase space theory calculations of rotational sums and densities of states.[45]

2. Density of transitional states

The expression for $\Omega_J(\epsilon)$ is

$$\Omega_J(\epsilon) = (2\pi)^{-8}\sigma^{-1}\int\cdots\int \times dJ_z\, dj_1\, dj_2\, dk\, dl\, d\kappa_1\, d\kappa_2\, d\alpha\, d\beta\, d\alpha_1\, d\alpha_2\, d\alpha_k\, d\alpha_l\, d\gamma_1\, d\gamma_2 \times\Delta(J,k,l)\Delta(k,j_1,j_2)\delta(\epsilon - H_{\rm cl}). \quad \text{(E1)}$$

The limits on the angle variables are 0 to 2π, the J_z integral is over the interval $(-J, J)$, the κ_i integrals are restricted by $|\kappa_i| \leqslant j_i$, and the angular momenta j_1, j_2, and l are restricted by the indicated triangle inequalities and by energy conservation. For $X_1\cdots X_2$ the Hamiltonian $H_{\rm cl}$ is written as

$$H_{\rm cl} = E_{r1} + E_{r2} + \frac{l^2}{2\mu R^2} + V_t(r_{mn},\theta_1,\theta_2), \quad \text{(E2)}$$

where μ is the reduced mass for relative motion of the X_1 and X_2 fragments, r_{mn} $(m,n = 1\text{–}4)$ denotes a 4×4 set of distances which, together with θ_1 and θ_2 are described in (3). When the X_i's are symmetric tops, each rotational energy E_{ri} of a fragment X_i has the simple form $J_i^2/2I_A + \kappa_i^2/2I_r$. (The case of asymmetric tops is described at the end of this Appendix). The principal moments of inertia (I_A, I_B, I_C) of a fragment are determined from its R-dependent equilibrium geometry (Appendix C). In the particular case of CH_3 fragments $I_A = I_B < I_C$, each CH_3 is an oblate symmetrical top with symmetry axis C and with $I_r = I_A I_C/(I_A - I_C) < 0$. However, Eq. (E2) and the subsequent development apply to asymmetric tops as well, with a different expression for the rotational energy E_{ri}. The relation between the action-angle variables and the internal coordinates for the particular case of the $C_2H_6 \rightarrow CH_3\cdots CH_3$ system is described in Sec. 3.

3. Internal coordinates

For a system such as $C_2H_6 \rightarrow 2\ CH_3$ the potential V_t is modeled to be a function of the r_{mn} $(m,n = 1,2,3,4)$, which are the separation distances between atoms (four per fragment) of the two fragments, and a function of the angle θ_i between the C–C axis and the symmetry axis z_i'' of fragment i $(i = 1,2)$. Some of these coordinates are identified in Fig. 4(b). The coordinates $r_{\rm CH}$ and $\alpha_{\rm HCH}$ which determine the CH_3 structure are implicitly included in the state counting in $N_V(E' - \epsilon)$. The reaction coordinate R, the angular momenta j_1, j_2, l, and the projections κ_1, κ_2 are depicted in Fig. 4(c) for this system.

The CH_3 structure determines the atomic position vectors $\mathbf{r}_n^{(i)''}$ in the fragment-fixed (x_i'', y_i'', z_i'') system. The vectors $\mathbf{r}_n^{(i)}$ are then obtained from $\mathbf{r}_n^{(i)''}$ by two successive applications of the inverse rotation matrix $\mathbf{A}^{-1}$ [29]:

$$\mathbf{r}_n^{(i)} = \mathbf{A}^{-1}(\alpha_i, \theta_{li}, \beta_i)\mathbf{A}^{-1}(\gamma_i, \theta_{\kappa_i}, 0)\mathbf{r}_n^{(i)''}. \quad \text{(E3)}$$

Here, β_i is the angle from the x axis to the line of nodes N_i' in Fig. 4(a) (the intersection of the xy and $x_i' y_i'$ planes), θ_{li} is the angle between the z and z_i' axes and α_i is the angle from N_i' to the x_i' axis. Again, the zero in Eq. (E3) indicates that the angle from the x_i' axis to the line of nodes N_i''' (the intersection of $x_i' y_i'$ and $x_i'' y_i''$ planes) is zero, θ_{κ_i} is the angle between the z_i' and z_i'' axes, and γ_i is the angle from N_i''' to the x_i'' axis. Some of these various angles are described in Fig. 4(a). The separation vector $\mathbf{R}$ is given by

$$\mathbf{R} = \mathbf{A}^{-1}(\alpha_l, 0, 0)\mathbf{R}^*, \quad \text{(E4)}$$

where $\mathbf{R}^*$ is a column vector with components $(R,0,0)$.

To express V_t, and hence $H_{\rm cl}$ in Eq. (E2) in terms of J, R, $r_{\rm CH}$, $\alpha_{\rm HCH}$, and the integration variables in Eq. (E2), one needs to express θ_1, θ_2, and the r_{mn}'s in terms of those variables. The coordinates $(R, \alpha_l, r_{\rm CH}, \alpha_{\rm HCH}, \alpha_i, \theta_{li}, \beta_i, \gamma_i, \theta_{\kappa_i})$ specify, in the body-fixed (x, y, z) system, the following quantities: $\mathbf{R}$, the orientation $\mathbf{e}_{z_i''}$ of the symmetry axis of X_i and the position vectors $\mathbf{r}_n^{(i)}$ of the four atoms $(n = 1,2,3,4)$ in $(CH_3)_i$ with respect to the center of mass of $(CH_3)_i$ $(i = 1,2)$. From the above quantities, the internal coordinates $\cos\theta_i = \mathbf{e}_{r_{cc}} \cdot \mathbf{e}_{z_i''} (i = 1,2)$ and $r_{mn} = |\mathbf{R} + \mathbf{r}_m^{(1)} - \mathbf{r}_n^{(2)}|$ $(m, n = 1,\ldots 4)$ are readily determined. R is fixed beforehand, α_l is a variable of integration, and $r_{\rm CH}$ and $\alpha_{\rm HCH}$ are each set equal to their R-dependent equilibrium values $r_{{\rm CH},e}$ and $\alpha_{{\rm HCH},e}$ (Appendix C).

The angles α_l, α_i, and γ_i in Eqs. (E3) and (E4) are defined in Table I; $\theta_{\kappa_i} = \cos^{-1}(\kappa_i/j_i)$; θ_{li} is defined in Table II; β_i, the angle between $\mathbf{l}\times\mathbf{k}$ [which lies along the x axis in Fig. 4(a)] and $\mathbf{N}_i' = (\mathbf{l}\times\mathbf{j}_i)$, is specified in the interval $(0, 2\pi)$ by Eqs. (E5) and (E6):

$$\cos\beta_i = [\cos\theta_{ki} - \cos\theta_{li}\cos\theta_{lk}]/[\sin\theta_{li}\sin\theta_{lk}]. \quad \text{(E5)}$$

Equation (E5) follows from Eq. (7) with **a**, **b**, **c**, **d** identified as in Table III. To determine the quadrant for β_i one can use a vector identity[46] and ultimately obtain

$$\sin\beta_i = \mp\sin\theta_{ki}\sin\alpha_k/\sin\theta_{li}, \quad \text{(E6)}$$

where the minus sign is for $i = 1$ and the plus sign for $i = 2$. The sign difference arises from the fact that $\mathbf{j}_1\times\mathbf{k} = -\mathbf{j}_2\times\mathbf{k}$. The conjugate angle α_k in Eq. (E6) is defined in Table I; the angles θ_{ki} and θ_{lk} in Eqs. (E5) and (E6) are defined in Table II.

$H_{\rm cl}$ is specified by the variables $(R, r_{\rm CH}, \alpha_{\rm HCH}, J, l, k, j_1, j_2, \kappa_1, \kappa_2, \alpha_k, \alpha_l, \alpha_1, \alpha_2, \gamma_1, \gamma_2)$ and is independent of (J_z, α, β). Equation (E1) now becomes

$$\Omega_J(\epsilon) = (2J+1)(2\pi)^{-6}\sigma^{-1}\int\cdots\int \times dj_1\, dj_2\, dk\, dl\, d\kappa_1\, d\kappa_2\, d\alpha_1\, d\alpha_2\, d\alpha_k\, d\alpha_l\, d\gamma_1\, d\gamma_2 \times\Delta(J,k,l)\Delta(k,j_1,j_2)\delta(\epsilon - H_{\rm cl}) \quad \text{(E7)}$$

and

$$N_{EJ} = (2J+1)(2\pi)^{-6}\sigma^{-1}\int\cdots\int \times dj_1\, dj_2\, dl\, dk\, d\kappa_1\, d\kappa_2\, d\alpha_1\, d\alpha_2\, d\alpha_k\, d\alpha_l\, d\gamma_1\, d\gamma_2 \times N_V(E' - H_{\rm cl})\Delta(J,k,l)\Delta(k,j_1,j_2). \quad \text{(E8)}$$

The evaluation of Eq. (E8) is described in Sec. III.

4. Asymmetric top case

We conclude this Appendix with a discussion of the asymmetric top case, to replace the expression given for E_{ri}

following Eq. (E2).

In the fragment-fixed (x_i'', y_i'', z_i'') frame in which the projection of $\mathbf{j}_i$ on the z_i'' axis is $\kappa_i = j_{iz''}$ and in which the inertia tensor is diagonal, the rotational energy of a rigid asymmetric top with principal moments $I_A \neq I_B \neq I_C$ is

$$E_{ri} = (j_{ix''}^2/2I_A) + (j_{iy''}^2/2I_B) + (j_{iz''}^2/2I_C). \tag{E9}$$

Unlike κ_i, $j_{ix''}$ and $j_{iy''}$ are not variables of integration in Eqs. (E7) and (E8) but are readily specified in terms of these variables by rotating the coordinate axes from the primed to the doubly primed system, i.e.,

$$\mathbf{j}_i'' = \mathbf{A}(\gamma_i, \theta_{\kappa i}, 0)\mathbf{j}_i', \tag{E10}$$

where $\mathbf{j}_i''$ and $\mathbf{j}_i'$ are column vectors with components $(j_{ix''}, j_{iy''}, j_{iz''})$ and $(0,0,j_i)$, respectively. Equation (E10) yields

$$j_{ix}'' = j_i \sin\theta_{\kappa_i} \sin\gamma_i,\ j_{iy}'' = j_i \sin\theta_{\kappa_i} \cos\gamma_i,\ j_{iz}'' = j_i \cos\theta_{\kappa_i}. \tag{E11}$$

We turn next to the value of the σ in Eq. (E8). When the CH_3's are planar, as they are in a loose transition state, the value of σ is $6\times6\times2 = 72$. When the transition state is more restricted, as at smaller $R^\dagger$'s, each CH_3 lies in a double-well potential for the out-of-plane H_3 vs C motion, and the stablest CH_3 configuration is now bent. For the case that the transition state is still nearly loose, we shall freeze each CH_3 in a bent configuration, count the phase space as before, and use $\sigma = 72$, thus ensuring that the phase space divided by σ is a continuous function of R at large R's. If the transition state were instead quite tight, one of the two wells of this double-well potential would disappear, and σ would equal 18, in the case of free internal rotation about the CC axis. An interpolation formula between these two limiting situations can be designed, or a more elaborate treatment for the out-of-plane CH_3 motion can be given. (For example, these two coordinates can be included in the transitional modes, and either treated classically or current path integral techniques can be used in the Monte Carlo calculations to treat them quantum mechanically, in the presence of the remaining classical-like transitional modes.) However, these refinements are omitted in the present paper.

APPENDIX F: MONTE CARLO CALCULATION OF N_{EJ}

1. N_{EJ}

The Monte Carlo evaluation of N_{EJ} is described in this Appendix using the reaction $C_2H_6 \rightarrow 2CH_3$ as an illustration. The calculations for $NO_2 \rightarrow NO + O$ and $H_2O_2 \rightarrow 2OH$ were analogous. To evaluate the 12-dimensional integral appearing in Eq. (E8), a 12-dimensional vector ξ is first defined whose components ξ_k are random numbers uniformly distributed on the interval (0, 1). In obtaining a particular ξ an additional random number was used to shuffle[13] the order in which the 12 numbers were obtained from a pseudorandom number generator, to avoid the possible repetitive assignment of correlated n-tuples to the same ξ_i's. The assignment of the action-angle variables in Eq. (E8) to the ξ_i's were as follows:

$$\begin{aligned} j_i &= \xi_i j_i^{\max}\ (i = 1,2), \\ k &= k^{\min} + (k^{\max} - k^{\min})\xi_3, \\ l &= l^{\min} + (l^{\max} - l^{\min})\xi_4, \\ \kappa_i &= 2j_i(\xi_{i+4} - 1/2),\ \alpha_i = 2\pi\xi_{i+6},\ \gamma_i = 2\pi\xi_{i+8}\ (i = 1,2), \\ \alpha_k &= 2\pi\xi_{11},\ \alpha_l = 2\pi\xi_{12}, \end{aligned} \tag{F1}$$

where $j_i^{\max}$ equals $[2I_C(R)E_{ri}^{\max}]^{1/2}$ for an oblate top $(I_C > I_A = I_B)$, with $E_{r1}^{\max} = E'$ and $E_{r2}^{\max} = E' - E_{r1}(j_1, \kappa_1)$; $k^{\min}$ is $|j_1 - j_2|$, $k^{\max}$ is $j_1 + j_2$, $l^{\min}$ is $|J - k|$, $l^{\max}$ is $\min[J + k, (2\mu R^2 E_l^{\max})^{1/2}]$, and $E_l^{\max}$ is $(E' - E_{r1} - E_{r2})$.

Introducing the transformation equation (F1) into Eq. (E8) yields

$$N_{EJ} = (2J+1)\int\cdots\int d\xi\, G(\xi), \tag{F2}$$

with $d\xi$ denoting $d\xi_1 \cdots d\xi_{12}$ and

$$\begin{aligned} G(\xi) = {} & j_1^{\max} j_2^{\max}(k^{\max} - k^{\min}) \\ & \times (l^{\max} - l^{\min}) 2j_1 2j_2 N_V(E' - H_{cl}) \\ & \times \theta(k^{\max} - k^{\min})\theta(l^{\max} - l^{\min}) \\ & \times \theta(|\kappa_1| - \kappa_1^{\min})\theta(|\kappa_2| - \kappa_2^{\min}). \end{aligned} \tag{F3}$$

The step functions θ for κ_1 and κ_2 are an additional restriction arising from the requirement that E_{ri} be nonnegative. For an oblate symmetric top and for a given j_i, this condition leads to $\kappa_i^{\min}$ being equal to $\{-2I_r(R)[E_{ri}^{\max} - j_i^2/2I_A(R)]\}^{1/2}$ if j_i is greater than $j_i^{\min} = [2I_A(R)E_{ri}^{\max}]^{1/2}$ and equal to 0 otherwise. (As noted in Appendix E, I_r is negative.) For other types of tops different restrictions apply. A Monte Carlo estimate for N_{EJ} in terms of $G(\xi)$ is

$$N_{EJ}^{MC} = (2J+1)\sum_{n=1}^{N} G(\xi_n)/N$$

with

$$\sigma^{MC} = \left\{ |(N_{EJ}^{MC})^2 - (2J+1)^2 \sum_{n=1}^{N} [G(\xi_n)]^2/N|/N \right\}^{1/2}, \tag{F4}$$

where N is the number of Monte Carlo points. Accumulated intermediate results for N_{EJ}^{MC} and σ^{MC} were examined at equally spaced increments of $\Delta n = N/10$ and provided a useful assessment of the convergence for a given N.

2. Variance reduction

When the number of rejected points in Eq. (F4), i.e., the number of terms with $G(\xi_n) = 0$ is reduced for a given N, the convergence of N_{EJ}^{MC} is improved. As a first step it was found that choosing j_1 and j_2 as the outer variables of integration in Eq. (E8), instead of l for example, significantly reduced σ^{MC}. The technique of uniform stratification[13] was next applied to the outer integration variable j_1. For subintervals of length $\Delta j_{1,k} = j_1^{\max}/5 (k = 1,2,\ldots 5)$ it was found that only a variance reduction of $\sim 10\%$ occurred when equal numbers of points $N_k = N/5$ were used in each subinterval, as compared to no stratification using the same number of integration points. More importantly, however, this procedure revealed orders-of-magnitude differences between contributions $N_{EJ,k}^{MC}$ to N_{EJ}^{MC} from some of the five subintervals. Those subintervals

with larger contributions were also found to have larger variances, making it clear that increasing the sampling of these bins relative to those with smaller contributions would decrease the overall variance for a given N.

In importance sampling, we recall, some weighting function is used for the sampling. In the case of the present integral with its complicated limits a weighting function for the integration variables was not immediately obvious. Instead, an empirical weighting function in histogram form was obtained for j_1 by preliminary uniform sampling, as above, and then that histogram was used in the importance sampling.[13]

To obtain an appropriate nonuniform random number distribution for j_1 the uniform stratification described above was used to provide approximate values of $N^{\mathrm{MC}}_{EJ,m}$. This procedure typically utilized $3\Delta n$ or $4\Delta n$ points of the total of $N(=10\Delta n)$ points. A cumulative distribution vector[13] $\{C_1, C_2,...\}$ for the bin values was obtained in histogram form:

$$C_k = \sum_{m=1}^{k} N^{\mathrm{MC}}_{EJ,m} \Big/ \sum_{m=1}^{5} N^{\mathrm{MC}}_{EJ,m} \quad (k = 1\text{–}5). \tag{F5}$$

The remaining $N - 4\Delta n$ or $N - 3\Delta n$ Monte Carlo integration points were chosen as follows: Together with each 12-component random number, an additional random number ξ_{13} uniformly distributed on (0, 1) was generated. The bin k of width $\Delta j_{1,k}$ to which j_1 was assigned was determined as the k for which $C_k > \xi_{13} > C_{k-1}$. The j_1 value was then chosen uniformly within this k th bin according to the random variable ξ_1; all other variables were selected in the manner described previously [cf. Eq. (F1)]. The next choice of $\xi_1,...,\xi_{13}$ was then made and the entire procedure repeated until the remaining $N - 4\Delta n$ or $N - 3\Delta n$ points were used.

3. N_V

For $NO_2 \rightarrow NO + O$, N_V was determined explicitly for each Monte Carlo point ξ_n. For the Morse oscillator model of the NO vibration, the classical vibrational energy E'_V in excess of the zero point energy in units of $\hbar = 1$ is $(4D/k^2)$ $[(x+\frac{1}{2})k - (x+\frac{1}{2})^2 - (\frac{1}{2})k + (\frac{1}{2})^2]$, where k is a dimensionless quantity (in units of $\hbar = 1$) $2\sqrt{2\mu D}/\beta$, μ is the NO reduced mass, the Morse parameters D and β are those in Appendix A, and $2\pi(x+\frac{1}{2})$ is the classical vibrational action,[11] x being a continuous variable, the classical equivalent of a "quantum number." This equation for $E'_V(x)$ is readily inverted to yield $x(E'_V)$. With E'_V equal $E' - H_{\mathrm{cl}}(\xi_n)$, the corresponding maximum vibrational quantum number $n^{\max}$ is the greatest integer less than or equal to x and the number of vibrational states with energy $E'_V < E' - H_{\mathrm{cl}}(\xi_n)$ is $N_V = n^{\max} + 1$.

For $H_2O_2 \rightarrow 2\,OH$, N_V was also determined explicitly for each Monte Carlo point ξ_n via the Morse oscillator model of the two OH vibrations (Appendix B). The vibrational quantum numbers of the OH bonds are the integers n_1 and n_2. The value of n_2 goes from zero to a maximum $n_2^{\max}$, obtained as the greatest integer for which E'_{V2}, the vibrational energy of this second bond in excess of its zero point energy, $< E' - H_{\mathrm{cl}}(\xi_n) - E'_{V1}(n_1)$. That is, $n_2^{\max}$ is a function of n_1. The maximum value of n_1, $n_1^{\max}$, is the greatest integer for which $E'_{V1} < E' - H_{\mathrm{cl}}(\xi_n)$. The total number of vibrational states N_V is the sum

$$\sum_{n_1=0}^{n_1^{\max}} [n_2^{\max}(n_1) + 1].$$

For $C_2H_6 \rightarrow 2\,CH_3$, the greater number of vibrational modes and the increased dimensionality of the N_{EJ} integral make a specific evaluation of N_V for each Monte Carlo point undesirable. N_V was determined as a function of E'_V before evaluating Eq. (E8) as follows. For the purpose of counting the vibrational states of the two identical CH_3 fragments there are, in total, two doubly degenerate modes with frequencies ν_1 and ν_2, and two quadruply degenerate modes with frequencies ν_3 and ν_4. These frequencies are assumed to depend on R as in Eq. (C2). Denoting the principal quantum numbers for these four modes by n_i $(i = 1\text{–}4)$ one can write the total vibrational energy E'_V in excess of the zero point energy as $2\pi(n_1\nu_1 + n_2\nu_2 + n_3\nu_3 + n_4\nu_4)$ in units of $\hbar = 1$. The corresponding degeneracy w is $w^{(2)}_{n_1} w^{(2)}_{n_2} w^{(4)}_{n_3} w^{(4)}_{n_4}$, where $w^{(d_i)}_{n_i}$ equals $(n_i + d_i - 1)!/n_i!(d_i - 1)!$ and d_i is the degeneracy of the ith oscillator.[47] All quartets (n_1, n_2, n_3, n_4) were determined such that $E'_V < E'$ and the corresponding degeneracy w was assigned to a linear array based on an energy grid of $\Delta E = 1\ \mathrm{cm}^{-1}$ (although in practice $10\ \mathrm{cm}^{-1}$ would undoubtedly have sufficed). The number of vibrational states $N_V(E'_n)$ with energy less than or equal to E'_n $(= n\Delta E)$ is given by the sum $\Sigma_{k=1}^{n} g_k$, where k is an array index: $g_k = 0$ if there is no vibrational state in the kth E'_V interval $[(k-1)\Delta E, k\Delta E]$, and g_k is the value of the sum of the degeneracies w for states in that interval ($g_1 = 1$ for the ground state). For each Monte Carlo point ξ_n, $N_V(E'_n)$ was simply read from the array with index determined from the value of $E'_n[= E' - H_{\mathrm{cl}}(\xi_n)]$. The grid size chosen is a compromise between computer memory requirement and the inaccuracy associated with multiple entries in the same array position (a very minor inaccuracy for a small grid size). Multiple entries appeared only at higher energies where vibrational levels are closely spaced. Analysis of the computational results for $C_2H_6 \rightarrow 2\,CH_3$ indicated that at low values of $\epsilon[= H_{\mathrm{cl}}(\xi_n)]$ and hence at high E'_V $(= E' - \epsilon)$ values, there was little contribution of multiple entries to N^{MC}_{EJ} for the (E, J) values used in the present study. For the largest E' (and hence E'_V) used, ~ 122 kcal mol^{-1}, approximately 4% of the array positions had multiple entries.

APPENDIX G: VARIABLE REDUCTION FOR $J = 0$ CASE

(a) $NO_2 \rightarrow NO + O$: If $J = 0$, then $\mathbf{j} = \mathbf{l} = 0$, $j = l$, and $\cos\theta_{lj} = -1$. That is the Δ in Eq. (8) becomes $\delta(j - l)$. Equation (6) becomes

$$\cos\gamma = \cos(\alpha_l + \alpha_j). \tag{G1}$$

The integrand is now independent of $\alpha_l - \alpha_j$. Writing $\theta_s = \frac{1}{2}(\alpha_l + \alpha_j) = \frac{1}{2}\gamma$, $\theta\omega_d = \alpha_l - \alpha_j$, and introducing the function $\delta(j - l)$ in Eq. (8), a two-dimensional integral is obtained. After integrating over the appropriate (θ_s, θ_d) domain[48] one obtains

$$\Omega_{J=0}(\epsilon) = (2\pi)^{-2}\int dj \int dl \int d\theta_s \int d\theta_d\ \delta(j-l)\delta(\epsilon - H_{\rm cl})$$
$$= 2(2\pi)^{-1}\int dj \int_0^{\pi} d\theta_s\ \delta(\epsilon - H_{\rm cl}). \qquad \text{(G2)}$$

The same property, namely that the integrand is independent of an angle θ_d, will be true in (b) and (c) also.

(b) $H_2O_2 \rightarrow 2OH$: if $J=0$, then $\mathbf{l}+\mathbf{k}=0$, $k=l$, $\cos\theta_{lk} = -1$, and $\cos\theta_{li} = -\cos\theta_{ki}$ $(i=1,2)$. The reference axis $\mathbf{x}$ for the angles of α_l and α_k (see Table I) is no longer defined since $\mathbf{l}\times\mathbf{k}=0$. Equation (D6) becomes

$$\cos\theta_R = \cos(\alpha_k + \alpha_l). \qquad \text{(G3)}$$

We redefine $\theta_R = \alpha_k + \alpha_l$ as the angle between $\mathbf{j}_1\times\mathbf{j}_2$ and $\mathbf{R}$ and $\theta_{ri} = \alpha_i$ as the angle between $\mathbf{j}_1\times\mathbf{j}_2$ and $\mathbf{r}_i$.

Equation (7) with $(\mathbf{a},\mathbf{b},\mathbf{c},\mathbf{d}) = (\mathbf{j}_1\times\mathbf{j}_2, \mathbf{r}_i, \mathbf{j}_1\times\mathbf{j}_2, \mathbf{R})$ yields

$$\cos\gamma_i = \cos\theta_R\cos\alpha_i + \sin\theta_R\sin\alpha_i\cos\theta_{li}. \qquad \text{(G4)}$$

Introducing the variables $\theta_s = \frac{1}{2}(\alpha_l + \alpha_k) = \frac{1}{2}\theta_R$ and $\theta_d = \alpha_l - \alpha_k$ and, for Δ, the function $\delta(l-k)$ in Eq. (D8) one obtains the six-dimensional integral

$$\Omega_{J=0}(\epsilon) = 2(2\pi)^{-3}\int\cdots\int$$
$$\times dj_1\, dj_2\, dk\, d\alpha_1\, d\alpha_2\, d\theta_s\ \Delta(k,j_1,j_2)\delta(\epsilon - H_{\rm cl}), \qquad \text{(G5)}$$

where α_1 and α_2 vary from 0 to 2π and θ_s varies from 0 to π.

(c) $C_2H_6 \rightarrow 2CH_3$: As for $H_2O_2 \rightarrow 2OH$ $k=l$, $\cos\theta_{lk} = -1$, $\cos\theta_{li} = -\cos\theta_{ki}$ $(i=1,2)$, and the reference axis $\mathbf{l}\times\mathbf{k}$ for α_l and α_k (see Table I) is again no longer defined. In addition the Euler angle β_i between $\mathbf{l}\times\mathbf{k}$ and $\mathbf{l}\times\mathbf{j}_i$ needs to be redefined. In the special case of $J=0$, $\mathbf{l} = -\mathbf{k}$ and so $\mathbf{l}\times\mathbf{j}_1 = \mathbf{j}_1\times\mathbf{k} = \mathbf{j}_1\times\mathbf{j}_2$ and $\mathbf{l}\times\mathbf{j}_2 = \mathbf{j}_1\times\mathbf{k} = \mathbf{j}_2\times\mathbf{j}_1$. From the definition of α_k in Table I, it is seen that α_k and β_1 now define rotations between the same axes in the xy plane. The sense of these rotations is opposite since β_1 is a rotation about the z axis which lies along $\mathbf{l}$ and α_k is a rotation about $\mathbf{k}$ which lies along $-\mathbf{l}$. This is verified by simplifying Eqs. (E5) and (E6) using $\cos\theta_{lk} = -1$, $\sin\theta_{lk} = 0$, and $\cos\theta_{ki} = -\cos\theta_{li}$, giving $\cos\beta_1 = \cos\alpha_k$ and $\sin\beta_1 = -\sin\alpha_k$, or $\beta_1 = -\alpha_k$. Similarly, it can be shown that $\beta_2 = \pi - \alpha_k$. The integrand depends on the angle between $\mathbf{R}$ and $\mathbf{j}_1\times\mathbf{j}_2$, namely, $\beta_1' = |\beta_1 - \alpha_l| = |-\alpha_k - \alpha_l| = \alpha_l + \alpha_k$. Introducing, therefore, the variables $\theta_s = \frac{1}{2}(\alpha_l + \alpha_k)$ and $\theta_d = \alpha_l - \alpha_k$ and the function $\delta(l-k)$ in Eq. (E7) yields the ten-dimensional integral

$$\Omega_{J=0}(\epsilon) = 2(2\pi)^{-5}\int\cdots\int$$
$$\times dj_1\, dj_2\, dk\, d\kappa_1\, d\kappa_2\, d\alpha_1\, d\alpha_2\, d\theta_s\, d\gamma_1\, d\gamma_2$$
$$\times\Delta(k,j_1,j_2)\delta(\epsilon - H_{\rm cl}), \qquad \text{(G6)}$$

where $\beta_1'(=2\theta_s)$ and β_2' $(=\pi+\beta_1')$ replace β_1 and β_2 in Eq. (E3) and where the x axis is now taken to lie along $\mathbf{R}$.

APPENDIX H: SOME RELEVANT NOTES ON THE PRESENT CALCULATIONS WITH SACM METHOD

The SACM method uses, as in RRKM theory, Eq. (1), but differs in the method for counting N_{EJ}. It is assumed that vibrationally adiabatic eigenvalues $E_a(q)$ can be found for any value of the reaction coordinate q by interpolating between reactant $(q=q_e)$ and product $(q=\infty)$ eigenvalues by a universal exponential interpolation function $g(q)$. Specifically, it is assumed that

$$E_a(q) = E_a(n_p,\infty)$$
$$+ [E_a(n_r,g_e) - E_a(n_p,\infty)]g(q) + E_{\rm cent}(q) + V(q), \qquad \text{(H1)}$$

where $V(q)$ is the potential along q, and n_p and n_r denote the totality of quantum numbers for motion transverse to q for products and reactants respectively; $E_{\rm cent}$ is a centrifugal term, assumed to be $P(P+1)/2\bar{I}(q)$, with P equal to $l + (J-l)g(q)$, l is the orbital angular momentum of the fragments, restricted to lie between $|J-j|$ and $J+j$, and $\bar{I}$ is the mean of the two larger principal moments of inertia of ON–O for a fixed bending angle. The interpolation function $g(q)$ and the Morse potential for $V(q)$ are given in Appendix A with q identified as the ON–O separation distance.

The reactant–product correlation in Eq. (H1) is subject to conservation of J and to vibrational adiabaticity for those modes whose quantum numbers are assumed to be conserved. In practice, product vibrations were correlated on a 1 : 1 basis with appropriate reactant vibrations. Only "adiabatic channels" whose eigenvalue maxima are less than the final asymptotic available energy are, or course, counted in N_{EJ}. Either symmetry-adapted counts can be made (i.e., correlating only states of the same symmetry) or all states can be counted and then corrected by introduction of approximate symmetry-correction factors.[19] In comparing the present method with SACM calculated results only total numbers of states were utilized and no symmetry corrections were introduced.

For the particular case of $NO_2 \rightarrow NO + O$, $E_a(n_p,\infty)$ was written (in units of $\hbar = 1$) as

$$E_a(n_p,\infty) = (4D_{\rm NO}/k_{\rm NO}^2)[(v+\tfrac{1}{2})k_{\rm NO} - (v+\tfrac{1}{2})^2] \qquad \text{(H2)}$$
$$+ [j(j+1)/2\mu_{\rm NO}r_e^2],$$

where n_p denotes the pair (v,j), $\mu_{\rm NO}$ is the reduced mass of NO, r_e is the equilibrium NO bond length, and $k_{\rm NO}$ equals $2(2\mu_{\rm NO}D_{\rm NO})^{1/2}/\beta_{\rm NO}$ in units of $\hbar = 1$. $E_a(n_r,q_e)$ was written as

$$E_a(n_r,q_e) = (4D_{\rm ON\text{-}O}/k_{\rm NO\text{-}O}^2)[(v+\tfrac{1}{2})k_{\rm ON\text{-}O} - (v+\tfrac{1}{2})^2]$$
$$+ (v_b + \tfrac{1}{2})h\nu_2 + (\kappa^2/2I_{re}), \qquad \text{(H3)}$$

where n_r denotes $(\mathrm{v}, \mathrm{v}_b, \kappa)$; ν_2 is the ONO bending frequency and the last term in Eq. (H3) denotes an "internal" rotational energy contribution to a prolate symmetric top model for NO_2 the restriction $|\kappa| \leqslant J$ is used. I_{re} equals $I_{Ae}\bar{I}_e/(\bar{I}_e - I_{Ae})$, where $\bar{I}_e$ is the arithmetic mean of I_{Be} and I_{Ce}. The three principal moments of inertia of NO_2 are listed in Table A1, together with other properties.

APPENDIX I: $F_\rho(E_r', J)$

An approximate correction factor $F_\rho(E_r', J)$ for rotation about the symmetry axis is readily obtained.[26(a)] For a symmetric top molecule with angular momentum projection K along the symmetry axis the rovibrational state density is

$$\rho_{vr}(E'_r, J) = (2J+1)\int_{-K_{max}}^{K_{max}} \rho_v\,[E'_r - E_{rot}(J,K)]\,dK, \tag{I1}$$

where E'_r is the total energy available to the reactant in excess of the zero point energy, the sum over K was replaced by the integral, and K_{max} is given below. For a prolate top such as ethane with $I_{A,r} = I_{B,r} > I_{C,r} E_{rot}$ equals $J^2/2I_{A,r} + K^2/2I_{r,r}$ (in units of $\hbar = 1$), where $I_{r,r} = I_{A,r}I_{C,r}/(I_{A,r} - I_{C,r})$ and $K_{max} = \min\{J, (2I_{r,r}x)^{1/2}\}$, and x denotes $E'_r - J^2/2I_{A,r}$. The integrand is an even function of K. Introduction of the Whitten–Rabinovitch approximation of ρ_v and making a change of variable from K to the variable $y = (K^2/2I_{r,r})/(x + aE_{Zr})$, one obtains[26(a)]

$$\frac{\rho_{vr}(E'_r,J)}{(2J+1)} = \frac{(x+aE_{Zr})^{s-1}}{\Gamma(s)\prod_{i=1}^{s} h\nu_i} \times\sqrt{2I_{r,r}(x+aE_{Zr})}\int_0^Y dy\, y^{-1/2}(1-y)^{s-1} \equiv \rho_v(x)F_\rho(x,J), \tag{I2}$$

where y equals $(K^2_{max}/2I_{r,r})/(x + aE_{Zr})$.

When K_{max} is determined by an energy requirement, namely that $K^2_{max} = (2I_{r,r}x)^{1/2}$, Y is close to unity. When, instead, J is very small, K_{max} equals J, Y is less than unity; typically only a little angular momentum was needed for the Y to be close enough to unity for the integral in Eq. (I2) to become the Beta function $B(\frac{1}{2}, s)$:

$$F_\rho \cong \sqrt{2I_{r,r}(x+aE_{Zr})}\,B(\tfrac{1}{2}, s). \tag{I3}$$

More generally, the integral in Eq. (I2) is $Y^{1/2}$ time the hypergeometric function $F(1-s, \frac{1}{2}; \frac{3}{2}; Y)$[49] and F_ρ can then be written as[49]

$$F_\rho(x,J) = \sqrt{2I_{r,r}(x+aE_{Zr})}\,2Y^{1/2} \times\left\{1 + \sum_{i=1}^{s-1} Y^i\left[\prod_{j=1}^{i}(j-s)\right]/(2i+1)i!\right\}. \tag{I4}$$

For a given rotational energy E'_r one can define a J_{max} as $\{2I_{A,e}E'_r\}^{1/2}$ and a J_{min} as $\{2I_{C,e}E'_r\}^{1/2}$. There are two cases to consider in evaluating the sum in Eq. (I4): (a) $0 < J < J_{min}$: In this case $K_{max} = J$ and so $Y = J^2/2I_{r,r}(x + aE_{Zr})^{-1}$, which is less then unity. (b) $J_{min} < J < J_{max}$: Here, $K_{max} = \{2I_{r,r}x\}^{1/2}$, which is less than J, and so $Y = x/(x + aE_{Zr})$. When x considerably exceeds aE_{Zr}, $Y \cong 1$ and Eq. (I3) is obtained, in agreement with a corresponding expression,[26(a)] when $B(\frac{1}{2}, s)$ is written in terms of gamma functions. Typical ratios of the value of F_ρ to that given by Eq. (I4) where 0.65, 0.95, and 1 when $J = 25$, 50, and 75 or greater, depending on the energy. For example, at $J = 25$, the ratio was 0.68 and 0.58 at $E'_\infty = 0.44$ and 63.5 kcal mol^{-1}, respectively. Typically, for the $C_2H_6 \rightarrow 2CH_3$ reaction at room temperature, the most probable of J is 25 and is higher at high temperatures.

The rotational factor F_ρ described above is for a microcanonical rate constant. Other rotational factors have been described for the thermal rate constant.[26(b),50]

[1] D. M. Wardlaw and R. A. Marcus, Chem. Phys. Lett. **110**, 230 (1984).
[2] R. A. Marcus, J. Chem. Phys. **20**, 359 (1952); R. A. Marcus and O. K. Rice, J. Phys. Colloid Chem. **55**, 894 (1951).
[3] See Ref. 1 and references cited therein.
[4] R. A. Marcus, J. Chem. Phys. **43**, 2658 (1965); **52**, 1018 (1970).
[5] E. Wigner, J. Chem. Phys. **5**, 720 (1937); Trans. Faraday Soc. **34**, 29 (1938); J. Horiuti, Bull Chem. Soc. Jpn. **13**, 210 (1938); J. C. Keck, J. Chem. Phys. **32**, 1035 (1960); Adv. Chem. Phys. **13**, 85 (1967); D. G. Truhlar, W. L. Hase, and J. T. Hynes, J. Phys. Chem. **87**, 2664 (1983), and references cited therein.
[6] See, for example, R. A. Marcus, J. Chem. Phys. **20**, 359 (1952); D. L. Bunker and M. Pattengill, *ibid.* **48**, 772 (1968); S. A. Safron, N. D. Weinstein, D. R. Herschbach, and J. C. Tully, Chem. Phys. Lett. **12**, 564 (1972); W. L. Hase and R. J. Wolf, J. Chem. Phys. **71**, 2911 (1979).
[7] D. M. Wardlaw and R. A. Marcus (in preparation).
[8] A. F. Turfa, D. E. Fitz, and R. A. Marcus, J. Chem. Phys. **67**, 4463 (1977).
[9] D. M. Wardlaw, Ph. D. thesis, University of Toronto, 1982.
[10] A. F. Wagner and E. K. Parks, J. Chem. Phys. **65**, 4343 (1976).
[11] In Ref. 1 the action variables were written as Nh, in units of $h = 1$, and the canonically conjugate angle variables covered a range (0, 1). In the present paper an equivalent choice is made in which the actions are $N\hbar$, in units of $\hbar = 1$, and the canonically conjugate angles cover an interval $(0, 2\pi)$.
[12] C. Kittel, W. D. Knight, and M. A. Ruderman, *Berkeley Physics Course* (McGraw–Hill, New York, 1965), Vol. 1.
[13] F. James, Rep. Prog. Phys. **43**, 1145 (1980).
[14] D. L. Bunker, J. Chem. Phys. **40**, 1946 (1964); S. C. Farantos, J. N. Murrell, and J. J. Hadjuk, Chem. Phys. **68**, 109 (1982).
[15] (a) J. D. Doll, Chem. Phys. Lett. **72**, 139 (1980); L. B. Bhuiyan and W. L. Hase, J. Chem. Phys. **78**, 5052 (1983); (b) J. Doll, *ibid.* **73**, 2760 (1980); **74**, 1074 (1981).
[16] D. W. Noid, M. L. Koszykowski, M. Tabor, and R. A. Marcus, J. Chem. Phys. **72**, 6169 (1980); M. V. Berry, Ann. Phys. **131**, 163 (1981).
[17] J. E. Adams, J. Chem. Phys. **78**, 1275 (1983).
[18] R. Viswanathan, L. M. Raff, and D. L. Thompson, J. Chem. Phys. **81**, 3118 (1984).
[19] M. Quack and J. Troe, Ber. Bunsenges. Phys. Chem. **78**, 240 (1974).
[20] W. L. Hase, J. Chem. Phys. **64**, 2442 (1976).
[21] R. J. Duchovic, W. L. Hase, B. Schlegel, M. J. Frisch, and K. Raghavachari, Chem. Phys. Lett. **89**, 120 (1982). These authors calculated an *ab initio* potential energy surface for the $CH_4 \rightarrow CH_3 + H$ reaction. The results indicated a deficiency similar to that discussed in the text, when a Morse model was fitted to the *ab initio* C–H bond-fission potential.
[22] For example, a Morse potential with β increasing by a factor 1.5 at $r - r_e = 3$ Å is known to represent the H_2 potential curve (Ref. 19), and an *ab initio* calculated stretching potential for $CH_4 \rightarrow CH_3 + H$ can be fitted by a Morse function with β represented by a cubic polynomial in $r - r_e$. [R. J. Duchovic and W. L. Hase, Chem. Phys. Lett **110**, 474 (1984)].
[23] This Varshni potential as a function of the ON–O distance x is $D\{1 - (x_e/x)\exp[-\beta(x^2 - x_e^2)]\}$. In the extensive comparative study of internuclear potential functions [D. Steele, E. R. Lippincott, and J. T. Vanderslice, Rev. Mod. Phys. **34**, 239 (1962)] the Varshni function was found to be one of three providing a superior description of the homo- and heteronuclear diatomics considered.
[24] R. J. Duchovic, W. L. Hase, and H. B. Schlegal, J. Phys. Chem. **88**, 1339 (1984).
[25] M. Quack, J. Phys. Chem. **83**, 150 (1979).
[26] (a) J. Troe, J. Chem. Phys. **79**, 6017 (1983); (b) J. Phys. Chem. **83**, 114 (1979).
[27] (a) W. Forst, *Theory of Unimolecular Reactions* (Academic, New York, 1973); (b) G. Z. Whitten and B. S. Rabinovitch, J. Chem. Phys. **38**, 2466 (1963).
[28] In classical trajectory calculations of the recombination rate constant for $H + CH_3 \rightarrow CH_4$ at $T = 300$ K the calculated rate increased by an order of magnitude when a Morse function rather than *ab initio* curve (Ref. 22) was used for the C–H stretching, perhaps because of the relatively low value of E'_∞ at 300 K.
[29] H. Goldstein, *Classical Mechanics* (Addison–Wesley, Reading, MA, 1950), $A^{-1}(\psi, \theta, \varphi)$ is given in Eq. (4-47) of p. 109.
[30] G. R. Bird, J. C. Baird, A. W. Jache, J. A. Hodgeson, R. F. Curl, A. C. Kunkle, J. W. Bransford, J. Rastrup-Anderson, and J. Rosenthal, J. Chem. Phys. **40**, 3378 (1964).
[31] G. Herzberg, *Electronic Spectra of Polyatomic Molecules* (Van Nostrand, New York, 1967).
[32] *JANAF Thermochemical Tables*, 2nd ed., NSRDS Natl. Bur. Stand. No.

37 (U. S. GPO, Washington, D.C., 1971).
[33]M. Quack and J. Troe, Ber. Bunsenges, Phys. Chem. **81**, 329 (1977).
[34]R. A. Bair and W. A. Goodard (private communication).
[35]T. Shimanouchi, J. Chem. Phys. Ref. Data **6**, 1018 (1977).
[36]P. Botschwina, W. Mayer, and A. M. Semkow, Chem. Phys. **15**, 25 (1976).
[37]*Tables of Bond Dissociation Energies for Simple Molecules*, NSRDS Natl. Bur. Stand. No. 31 (U. S. GPO, Washington, D.C., 1970).
[38]T. H. Dunning and N. W. Winter, J. Chem. Phys. **63**, 1847 (1975), and references cited therein.
[39]P. A. Giguere, in *Complements au Nouveau Traite de Chimie Minerale*, edited by P. Pascal (Masson et Cie, Paris, 1975), Vol. 4.
[40]G. Herzberg, *Spectra of Diatomic Molecules* (Van Nostrand, New York, 1950).
[41]J. Troe, J. Phys. Chem. **88**, 4375 (1984).
[42]A. Warshel, in *Semiempirical Methods of Electronic Structure Calculation, Part A: Techniques*, edited by G. A. Segal (Plenum, New York, 1977).
[43]W. A. Goddard (private communication).
[44]I. Kakagawa and T. Shimanouchi, J. Mol. Spectrosc. **39**, 255 (1971), (cf. set A in Table VII there.)
[45]W. J. Chesnavitch and M. T. Bowers, J. Chem. Phys. **66**, 2306 (1977).
[46]The following identity is used: $(\mathbf{a}\times\mathbf{b})\times(\mathbf{c}\times\mathbf{d}) = [\mathbf{a}\cdot(\mathbf{b}\times\mathbf{d})]\,\mathbf{c} - [\mathbf{a}\cdot(\mathbf{b}\times\mathbf{c})]\,\mathbf{d}$ with $\mathbf{a}=\mathbf{c}=\mathbf{l}$, $\mathbf{b}=\mathbf{k}$, $\mathbf{d}=\mathbf{j}_i$. One thus finds $\sin\beta_i = \cos\theta_{ix}/\sin\theta_{li}$, where θ_{ix} is the angle between $\mathbf{j}_i$ and $\mathbf{l}\times\mathbf{k}$. The above vector identity with $\mathbf{a}=\mathbf{l}$, $\mathbf{b}=\mathbf{d}=\mathbf{k}$, and $\mathbf{c}=\mathbf{j}_i$ yields $\cos\theta_{ix} = \mp\sin\theta_{ki}\sin\alpha_k$. Equation (E7) of the text follows from the last two results.
[47]M. Tinkham, *Group Theory and Quantum Mechanics* (McGraw–Hill, New York, 1964), p. 246.
[48]R. K. Pathria, *Statistical Mechanics* (Pergamon, Oxford, 1972), pp. 459–460.
[49]I. S. Gradshteyn and I. W. Ryzhik, *Table of Integrals, Series and Products* (Academic, New York, 1965), pp. 1039–1040.
[50]E. V. Waage and B. S. Rabinovitch, Chem. Rev. **70**, 377 (1970).